ASTROBIOLOGY
Volume 22, Number 6, 2022

DOI: 10.1089/ast.2021.0061

Characterization of the Halochromic Gloeocapsin Pigment, a Cyanobacterial Biosignature for Paleobiology and Astrobiology

Yannick J. Lara,[1] Andréa McCann,[2] Cédric Malherbe,[2] Camille François,[1,*] Catherine F. Demoulin,[1] Marie Catherine Sforna,[1] Gauthier Eppe,[2] Edwin De Pauw,[2] Annick Wilmotte,[3] Philippe Jacques,[4] and Emmanuelle J. Javaux[1]

Abstract

Ultraviolet (UV)-screening compounds represent a substantial asset for the survival of cyanobacteria in extreme environments exposed to high doses of UV radiations on modern and early Earth. Among these molecules, the halochromic pigment gloeocapsin remains poorly characterized and studied. In this study, we identified a gloeocapsin-producing cultivable cyanobacteria: the strain *Phormidesmis nigrescens* ULC007. We succeeded to extract, to partially purify, and to compare the dark blue pigment from both the ULC007 culture and an environmental *Gloeocapsa alpina* dominated sample. FT-IR and Raman spectra of *G. alpina* and *P. nigrescens* ULC007 pigment extracts strongly suggested a common backbone structure. The high-pressure liquid chromatography-UV-MS/MS analysis of the ULC007 pigment extract allowed to narrow down the molecular formula of gloeocapsin to potentially five candidates within three classes of halochromic molecules: anthraquinone derivatives, coumarin derivatives, and flavonoids. With the discovery of gloeocapsin in *P. nigrescens*, the production of this pigment is now established for three lineages of cyanobacteria (including *G. alpina, P. nigrescens*, and *Solentia paulocellulare*) that belong to three distinct orders (Chroococcales, Pleurocapsales, Synechoccocales), inhabiting very diverse environments. This suggests that gloeocapsin production was a trait of their common ancestor or was acquired by lateral gene transfer. This work represents an important step toward the elucidation of the structure of this enigmatic pigment and its biosynthesis, and it potentially provides a new biosignature for ancient cyanobacteria. It also gives a glimpse on the evolution of UV protection strategies, which are relevant for early phototrophic life on Earth and possibly beyond. Key Words: Cyanobacteria—Gloeocapsin—UV-screening—Halochromic—Pigment. Astrobiology 22, 735–754.

1. Introduction

Pigments represent attractive molecular tracers (or biosignatures) to probe Life in Time and Space. Indeed, their chemical complexity is not replicated by abiotic processes, they can be preserved in the geological record (up to at least 1.73 Ga) (Vinnichenko *et al.*, 2020), and they are produced by members of the three domains of life for the use of photons during phototrophy or as protective sunscreens. Taxonomic and functional specificities of these biomarkers are also essential to calibrate the tree of Life and to date evolutionary processes.

Among pigment-producing microorganisms, cyanobacteria are known to produce different classes of ultraviolet

[1]Early Life Traces & Evolution–Astrobiology, UR Astrobiology, University of Liège, Liège, Belgium.
[2]MolSys Research Unit, Mass Spectrometry Laboratory, University of Liège, Liège, Belgium.
[3]BCCM/ULC Cyanobacteria Collection, InBios-CIP, Institut de Chimie B6a, University of Liège, Liège, Belgium.
[4]Microbial Processes and Interactions, Gembloux Agro-Bio Tech, TERRA Teaching and Research Centre, Joint Research Unit BioEcoAgro UMRt 1158, University of Liège, Gembloux, Belgium.
*Present address: Commission for the Geological Map of the World, Paris, France.

(UV)-screening compounds, which include carotenoids, mycosporine-like amino acids, scytonemins, and gloeocapsins (Garcia-Pichel and Castenholz, 1991; Garcia-Pichel *et al.*, 1993; Hirschberg and Chamovitz, 1994; Castenholz and Garcia-Pichel, 2012; Storme *et al.*, 2015).

Chlorophyll and carotenoid derivatives are commonly used as biomarkers in Holocene (last 10 Ka) lacustrine paleoecology (Sanger, 1988), and they were recently extracted from a mid-Proterozoic (ca. 1.1 Ga) sedimentary sequence from the Taoudeni Basin in Mauritania (Gueneli *et al.*, 2018) and from the 1.64 and 1.73 Ga sequences of the McArthur basin in Australia (Vinnichenko *et al.*, 2020). These carotenoid derivatives could indicate the presence of cyanobacteria and/or green sulfur bacteria. Moreover, the isotopic characterization of nitrogen within 1.1 Ga porphyrins suggested a cyanobacterial origin.

To our knowledge, this is the oldest evidence for the presence of a cyanobacterial pigment in the fossil record. Nevertheless, Golubic and Hofmann (1976) suggested that the darker outer cell layer of the *Eoentophysalis* colonies ($\sim$1.9 Ga) could indicate the presence of pigments, but this was only based on microscopic observations. Green-sulfur, purple-sulfur bacteria and cyanobacterial pigments were also reported from the 1.6 Ga McArthur Group, Australia (Brocks *et al.*, 2005). Cyanobacterial lipids and pigments may be preserved not only in fossil oil, but also in association with recalcitrant biopolymers of polysaccharidic sheaths abundantly found in Precambrian fossil and modern cyanobacterial mats (Pawlowska *et al.*, 2013; Lepot *et al.*, 2014; Blumemberg *et al.*, 2015).

Scytonemins are the more extensively characterized extracellular cyanobacterial UV-screening pigments (Garcia-Pichel and Castenholz, 1991; Proteau *et al.*, 1993). They are indole-alkaloid extracellular pigments associated with polysaccharide sheaths, which protect cyanobacterial cells from UVA exposure (Proteau *et al.*, 1993). The biosynthesis of this pigment is ensured by the expression of a conserved cluster of genes, which delivers precursors of scytonemin (Soule *et al.*, 2007; Garcia-Pichel, *et al.*, 2019).

Hitherto, at least six molecular variants of scytonemin were characterized (Grant and Louda, 2013). Among them, the scytonemin-3a-imine, a reddish mahogany pigment, was compared with the enigmatic UV-screening gloeocapsin (Grant and Louda, 2013). Scytonemin is widespread across the cyanobacterial lineage, which suggests that this pigment may have already been produced by a common ancestor (Garcia-Pichel and Castenholz, 1991). Recent phylogenetic analyses and molecular dating of scytonemin gene clusters suggest a Precambrian origin of this UV-screening pigment (Garcia-Pichel *et al.*, 2019). The oldest record of scytonemin reported so far within microfossils was detected in brown cyanobacterial sheaths from ca. 4530-year-old fossilized mats collected in Antarctic lakes (Lepot *et al.*, 2014).

The pigmented sheaths were shown to be resistant to acid demineralization (HCl-HF) used for microfossil isolation in older rocks, and their Raman spectra were compared with those of strains (*Calothrix* sp. BCCM/ULC039). However, as non-pigmented sheaths were also preserved, scytonemin likely played little role in the preservation of the polysaccharides, which appeared to be cross-linked by ether bonds.

Coccoidal fossils preserved thylakoids and autofluorescence of pigments such as carotenoids. These fossil pigmented sheaths, internal membranes, and pigments form diagnostic biosignatures of phototrophy and of cyanobacteria that could be looked for in the older fossil record (Demoulin *et al.*, 2019). Bulk extracts analyzed with high-pressure liquid chromatography (HPLC) suggested the presence of scytonemins and a ''scytonemin-like'' pigment in 125-Kyr-old Antarctic lacustrine sediments (Hodgson *et al.*, 2006).

Unlike scytonemins, the structure and biosynthesis pathway of the gloeocapsin have yet to be characterized. This lack of knowledge is mainly explained by the absence of cultivated gloeocapsin-producing strains, and thus, the impossibility to produce large amounts of purified molecules (Grant and Louda, 2013). The diagnosis of gloeocapsin was only based on the capacity of the sheath pigmentation to change color with pH, ranging from blue and violet in alkaline conditions to red in an acidic environment (Jaag, 1945; Büdel and Henssen, 1988; Radtke and Golubic, 2011; Pentecost and Whitton, 2012).

Nägeli and Schwenderer (1877) were the first to observe and name the pigment after the taxon *Gloeocapsa* spp. Similar halochromic changes in sheath pigmentation were also reported in several cyanobacterial species from at least two different orders (Chroococcales, Pleurocapsales) (Storme *et al.*, 2015). So far, a number of gloeocapsin-producing taxa were reported from different biotopes. They include two marine intertidal euendolithic Pleurocapsales, *Hyella pyxis* (Lukas and Hoffman, 1984) and *Solentia* spp., and *Hormathonema violaceum*, a marine epilithic cyanobacterium of the rocky intertidal zone (Radtke and Golubic, 2011).

Gloeocapsin was also found in epilithic communities of limestone walls in Europe (Storme *et al.*, 2015), in endolithic *Gloeocapsa* from gypsum (Němečková *et al.*, 2021), in rocky littoral of freshwater lakes in Europe (Pentecost, 2014), in rocky substrates of shallow streambeds and ponds in polar environments (Vincent, 2000), and in the lichen *Euopsis granatina* (Büdel and Henssen, 1988). The first and only spectroscopic characterization of gloeocapsin was performed *in vivo* by Raman microspectroscopy on colonies of *Gloeocapsa alpina* and *Solentia paulocellulare* (Storme *et al.*, 2015).

In their study, the authors compared the pigment in both acidic and alkaline conditions with the UVA screening scytonemin, and with published spectra obtained from an arctic cyanobacterial community growing on gypsum, dominated by *Gloeocapsa* and *Nostoc* colonies (Edwards *et al.*, 2005). They concluded on the presence of parietin in *G. alpina* polysaccharide sheath. In other cases, other anthraquinone derivatives are known to be produced by the freshwater cyanobacterium *Eucapsis* sp. and cyanobacteria-associated streptomycetes (Socha *et al.*, 2006; Sturdy *et al.*, 2010). In both cases, anthraquinone derivatives showed promising antibacterial effects.

Phormidesmis nigrescens, a recently revised thin filamentous cyanobacterium of the order Synechococcales with barrel-shaped cells, is characterized by its ability to produce a dark blue/purplish pigmented polysaccharidic sheath (Raabová *et al.*, 2019). This pigmentation was assigned to gloeocapsin, as it showed a halochromic shift after application of a Perényi solution (4% nitric acid, 0.15% chromic acid, 30% alcohol final concentrations), an acidic treatment used for fast dissolution of rocky substrates (Lamprinou *et al.*, 2013).

The strain *Phormidium priestleyi* ANTL52.4 aka ULC007, isolated from an Antarctic pond in the Larsemann Hills (Taton *et al.*, 2006), is phylogenetically related to the clade of *P. nigrescens* (Raabová *et al.*, 2019). However, the production of an extracellular pigment and exopolysacharidic sheath was not previously reported for the strain ULC007. Moreover, although the gloeocapsin pigment seems unique to cyanobacteria, it has never been isolated to further characterize its chemistry, role, and phylogenetic occurrence.

In this study, we report the production of a halochromic pigment in a new order of cyanobacteria (Synechococcales), represented by the strain ULC007, and the isolation, purification, and spectroscopic and spectrometric characterization of this compound that we compare with the enigmatic halochromic pigment produced by *G. alpina*: the gloeocapsin.

2. Materials and Methods

2.1. Environmental sample and culture growth

Environmental samples dominated by *G. alpina* were collected from the epilithic community of the limestone wall at Pont de Bonne, Hoyoux Valley, Modave, Belgium (50°28′27"N, 5°23′05"E) as described by Storme *et al.* (2015). Dark areas of microbial epilithic communities were scratched from the wall and stored at −20°C until extraction.

Non-axenic *P. priestleyi* ULC007 strain was obtained from the Belgian Co-ordinated Collection of Micro-organisms/ University of Liège Collection of cyanobacteria (BCCM/ULC) and was grown in BG11 medium (Rippka *et al.*, 1979) under constant white LED illumination (5–20 μmol photon m^{-2} s^{-1}) at 18°C. As ULC007 is an Antarctic slow-growing strain (Biondi *et al.*, 2008), its culture was incubated during 1 year to collect enough dark biomass.

2.2. Pigment extraction and purification

P. priestleyi ULC007 cells were harvested after centrifugation at 1610 *g* for 15 min. The resulting pellet was suspended in NaOH 1 *M*. In parallel, 5 g of the dark epilithic community were suspended in NaOH 1 *M*. Both NaOH suspensions were heated in a boiling water bath for 30 min, and they were autoclaved at 121°C for 20 min. Lysates were then centrifuged and precipitated in methanol: ethyl acetate (1:1), and colored fractions were collected and purified in chloroform: ethyl acetate: ethanol (1:1:1). Finally, the pigment fraction was centrifuged, dried, washed in absolute ethanol, and dried for spectroscopic and spectrometric analyses.

2.3. UV-visible spectroscopy

Dried pigment flakes were re-suspended in 100 μL of saline solution of K_2HPO_4 (20 g/L) plus Na-EDTA (0.05 g/L). To analyze the acid and basic form of the pigment, the pH of the solution was adjusted either to pH ∼2 using HCl 10% (acidic solution) or to pH ∼9 using NaOH 1 *M* (basic solution). The absorption spectra of both acidic and basic solutions were analyzed by using a TECAN Infinite M200PRO plate reader in a UV-Star 96-well microplate (Greiner Bio-One, NC).

2.4. Fourier-Transform InfraRed microspectroscopy

Dried flakes of extracted pigment were resuspended in 10 μL milliQ water. Spectral analysis was performed in the 4000–600 cm^{-1} range with the co-addition of 1024 scans at a spectral resolution of 4 cm^{-1} by using a Hyperion 2000 Bruker microscope coupled to a Tensor 27 FT-IR spectrometer (Bruker, MA) for gloeocapsins and 256 scans for reference pigments. Data were collected with a conventional Globar source equipped with 15× objective (NA = 0.4) and a liquid nitrogen-cooled MCT-A detector. Spectra acquisitions and baseline correction were collected and analyzed with the OPUS 8.0 software (Bruker).

2.5. Raman microspectroscopy

Dried pigment flakes were re-suspended in 100 μL of saline solution of K_2HPO_4 (20 g/L) plus Na-EDTA (0.05 g/L). The pH was adjusted as described in the earlier section; then drops of both acidic and basic solutions were deposited onto ZnSe windows and dried for 24 h in ambient air. Raman spectroscopy was performed by using a Renishaw inVia Raman spectrometer coupled to a Leica DM 2500 confocal microscope. Excitation was performed by using an Ar-ion-40 mW monochromatic 514 nm laser source and was adjusted at an intensity of maximum ca. 2 mW and focused through 50× (numerical aperture = 0.83) and 100× (numerical aperture = 0.74) objectives following the protocol described by Storme *et al.* (2015). Acquisitions were obtained with an 1800 L/mm grating with an air-cooled (−70°C) 1040×256-pixel CCD array detector. No thermal degradation of the sample was observed. Typically, the samples are interrogated with a laser power of ∼0.4 mW on the sample, and the spectrum stability is checked. If the spectrum fluctuates (*i.e.*, variation of intensity ratio or disappearance of signal), then the samples are interrogated with lower laser power (∼0.04 mW).

Spectra acquisition was performed with the Wire 5.1 software (Renishaw, United Kingdom), and data treatment was processed by a dedicated R routine based on HyperSpec R package (Beleites and Sergo, 2021).

To evaluate the distribution of the gloeocapsin in a *G. alpina* colony from Pont De Bonne and in a pigmented sheath of the cyanobacterium ULC007, two Raman maps were performed by using the high-resolution dynamic line-scanning Raman mapping approach via the Renishaw HR StreamLine mode and the 514 nm monochromatic Ar-ion-40 mW laser source. Resulting maps (hyperspectral matrices of 4608 spectra large for *G. alpina*, and of 989 spectra large for ULC007) were processed by using HyperSpec R package. Briefly, baselines were corrected by using a polynomial fitting approach using the function *spc.fit.poly.below* and intensity vectors were normalized. To assign vibrational bands to carotenoids and gloeocapsins, datasets were analyzed by using a « R-mode » hierarchical cluster analysis (R-HCA) as described by Bonifacio *et al.* (2015).

Briefly, Pearson squared distance matrices were constructed by using the function *pearson.dist* and Ward method to compute the dendrogram with the function *hclust* from *stats* package. Hyperspectral data were clustered into $k = 3$ clusters. Mean and standard deviation spectra were computed for each cluster by using the *aggregate* function from HyperSpec.

2.6. High-pressure liquid chromatography-UV-MS

To characterize the ULC007 putative gloeocapsin chromophores, an HPLC separation was performed, coupled with an UV and MS (electrospray ionization [ESI] ionization) detection system. An acidic extract of ULC007 (pink) was dried in a speed vacuum and resuspended in liquid chromatography–mass spectrometry (LCMS)-grade acetonitrile solvent. The HPLC separation was conducted on a Waters ACQUITY I-class instrument. Two HPLC mobile phases corresponding to milliQ water with 0.1% formic acid (eluent A), and to LCMS-grade acetonitrile with 0.1% formic acid (eluent B) were prepared.

The HPLC separation of the extract was performed in reverse-phase mode with a Waters ACQUITY C18 CSH column with a length of 150 mm, an inner diameter of 1 mm, and a particle size of 1.7 μm. The flow rate was set to 0.1 mL/min, the column temperature was set at 40°C, and the sample injection volume was set to 3 μL. The HPLC gradients of HPLC separation are given in Supplementary Table S1. A tunable UV detector (Acquity TUV waters), equipped with an analytical flow cell, was added post-column in single wavelength detection mode, at 256 nm (corresponding to the maximum UV absorbance of the colored extract in acidic conditions) with a sampling rate of 20 Hz.

A timsTOF mass spectrometer (Bruker Daltonik GmbH, Bremen, Germany) operating in positive ionization mode and scanning from *m/z* 100 to *m/z* 1300 with a resolution of 35,000 full width at half-maximum at 400 *m/z* was used for MS and MS/MS analysis, post-UV detection. MS/MS spectra were recorded with a collision energy of 40 eV. MS/MS spectra were recorded with a collision energy of 40 eV, and the isolation width was set to 1.0 Da. The capillary was held at 3.5 kV, and the source temperature was set to 180°C. Chromatograms and mass spectra were processed and analyzed by using DataAnalysis 5.0 software (Bruker Daltonik GmbH).

Putative molecular formulas were assigned to the detected ions by using the DataAnalysis SmartFormula algorithm, based on mass accuracy and isotopic abundances similarities (named as mSigma). This means that our molecular formulas are determined taking the contribution of the isotopic abundance of each element in the molecule into account to calculate the exact (accurate) mass of the compounds. Molecular formulas were searched considering naturally occurring adducts in the ESI positive ionization mode ($M+H^+$, $M+Na^+$, and $M+K^+$).

All putative molecular formulas showing a mSigma value comprised within the 5% isotopic abundance pattern error defined by Kind and Fiehn (2007) (*i.e.*, estimated at 50 mSigma) were considered. Finally, several supplementary criteria were added to ensure a correct molecular assignment: (1) mass accuracy should be below 5 ppm, (2) double bound equivalent must be an integer value, (3) nitrogen rule (stating that any molecule with all paired electrons and an odd number of nitrogen atoms will have an odd nominal mass) must be respected, (4) oxygen/carbon ratio must be equal or below 1, (5) nitrogen/carbon ratio must be equal or below 1, and (6) hydrogen/carbon ratio must be higher than 0.3.

Criteria 5 and 6 expressed that stoichiometry is relevant to biological compounds. In addition to the commonly used elemental composition ($C_{0-\infty}H_{0-\infty}O_{1-\infty}N_{0-\infty}$), Cl_{0-1}, Mg_{0-1}, and Fe_{0-1} were added to the predefined composition search, based on their known occurrence in cyanobacterial metabolites (Gademann and Portmann, 2008). Cell cultures, pigment extraction and purification, and Raman and FT-IR microspectroscopy were performed in the Early Life Traces & Evolution-Astrobiology Laboratory (UR Astrobiology, ULiege); UV-visible spectroscopy was conducted in the Centre d'Ingénierie des Protéines-CIP (UR InBios, ULiege); and HPLC-UV-MS was performed in the Mass Spectrometry Laboratory (UR Molsys, ULiege).

3. Results

The strain ULC007 is a narrow filamentous cyanobacterium with barrel-shaped cells that have a mean diameter of 1.4 μm (1.1–1.8 μm) and a mean length of 1.7 μm (1.3–2.3 μm). In young cultures, sheaths are absent, colorless, or invisible (Fig. 1); whereas in old cultures, conspicuous dark blue/purplish sheaths develop. We observed a color shift of the pigment from dark blue to red by adding a drop of a solution of 1% HCl or 10% acetic acid to the cell preparation under the microscope. The color change was also tested and observed for ULC007 empty sheaths and environmental *G. alpina* samples. In addition, we observed the accumulation of an extracellular pigment in the culture media of ULC007 (Fig. 1).

After boiling and autoclaving the culture and environmental biomass, we extracted and partially purified, through subsequent liquid–liquid washing in apolar solvents, the dark blue pigment from both the ULC007 culture and the environmental sample dominated by *G. alpina*. The dark blue pigment remained in the pellet or precipitated during the entire extraction process. After acidification in 30% HCl and resuspension in 75% methanol, the pigment turned red and became soluble.

At neutral pH, both purified pigment extracts were purple. The solutions shifted to red at low pH values and back to dark blue at high pH values, suggesting that the chromophore properties of the molecule were conserved as the halochromic behavior of the extracted molecules was retained after the extraction process (Fig. 2a).

The UV-visible absorbance spectra were measured for both extracts in acidic, neutral, and alkaline pH conditions. For the ULC007 extract, two absorbance peaks were observed for each spectrum (Fig. 2b). The first maximum of absorption occurred in the UV range of wavelengths, and it was observed at 256 and 258 nm at pH = 2 and pH = 11, respectively. The second peak of absorption occurred in the visible wavelength region, between 400 and 750 nm, and was observed at 492 nm at pH = 2, and at 585 nm at pH = 11 (Table 1).

The dark blue color of the pigment in alkaline pH arises from the absorption of the red and orange wavelengths in the visible region (typically between 660 and 580 nm), whereas the reddish/pink color of the pigment can be explained by the absorption of green wavelengths (typically between 500 and 580 nm) in acidic conditions. Although absorption bands were less intense for the spectra of the environmental *G. alpina* extracts, the position and shape of the bands seem to coincide with the position and shape of the bands observed for the ULC007 pigment. As observed for the ULC007

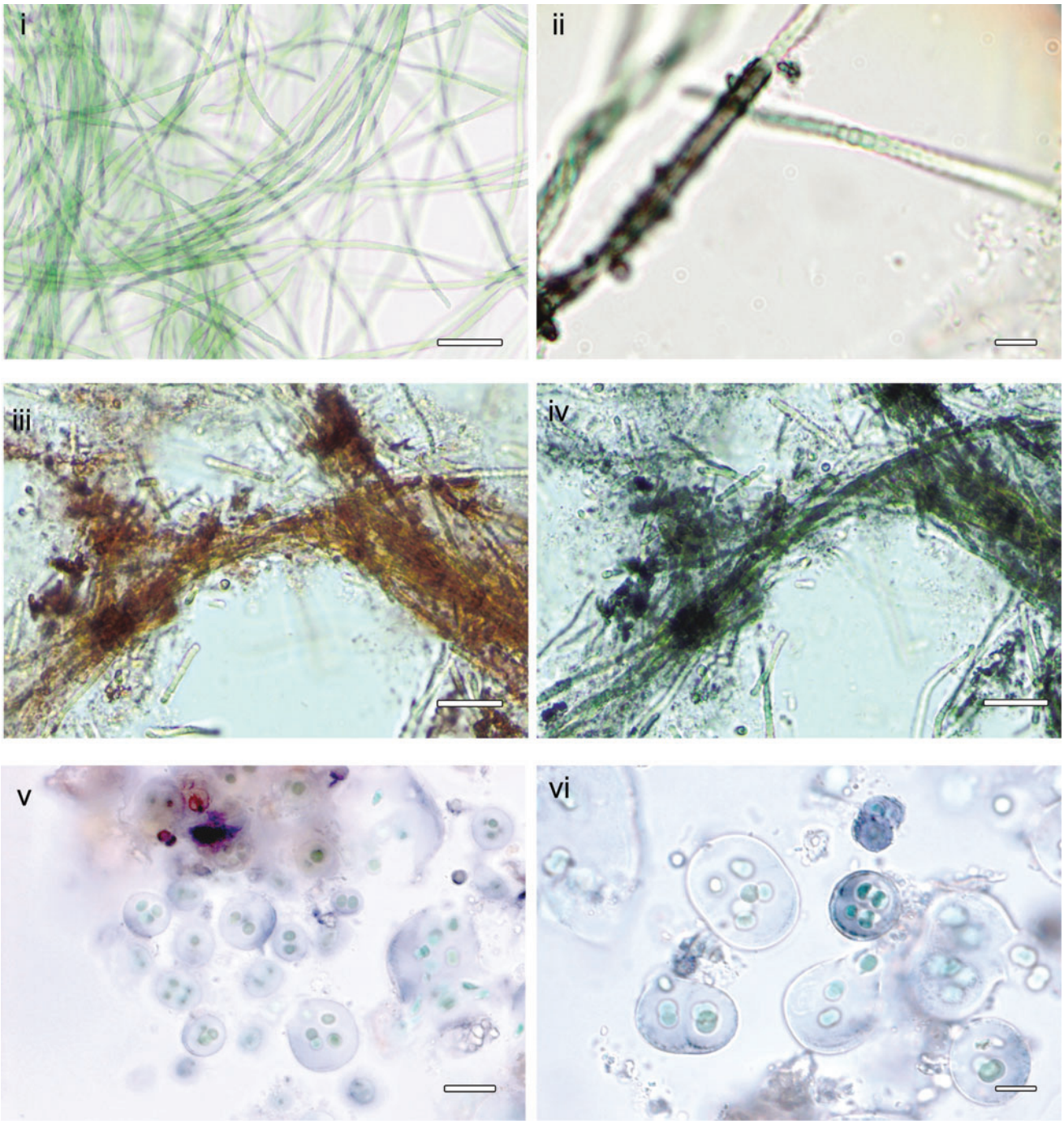

FIG. 1. Microphotographs of *Phormidesmis nigrescens* ULC007 and *Gloeocapsa alpina* of Pont de Bonne limestone wall. **(i)** Early stage culture of *P. nigrescens* ULC007 (scale 20 µm), **(ii)** dark sheathed filament of *P. nigrescens* ULC007 (scale = 5 µm), Old culture of *P. nigrescens* ULC007 **(iii)** in acidic (scale = 20 µm) and **(iv)** alkaline conditions, Environmental sample dominated by *G. alpina* **(v)** in acidic (scale = 20 µm) and **(vi)** alkaline conditions (scale = 10 µm). Color graphics are available online.

extract, the absorption bands observed for *G. alpina* were located at 504 nm in acidic pH and 582 nm in alkaline pH.

The pigmented extracts were also analyzed by FT-IR microspectroscopy. Although the spectrum obtained for the *G. alpina* extract is more complex due to the environmental origin of the sample, both *G. alpina* and ULC007 spectra showed five main common absorption bands (Fig. 3 and Table 2). For the ULC007 extract, a large band with a maximum absorption at 3395 cm^{-1} suggests that the extracts contain O-H functions. Between 1000 to 1800 cm^{-1}, a moderate peak at 1667 cm^{-1} is attributed to aromatic C = C stretching vibration and can also be assigned to a C = O stretching.

Two strong absorption peaks at 1561 and at 1417 cm^{-1} could be assigned to the aromatic ring breathing vibration mode, to C–N stretching, N–H deformation, or C–H deformation. However, there is no clear evidence of any absorption band at 3500 cm^{-1} attributable to N–H

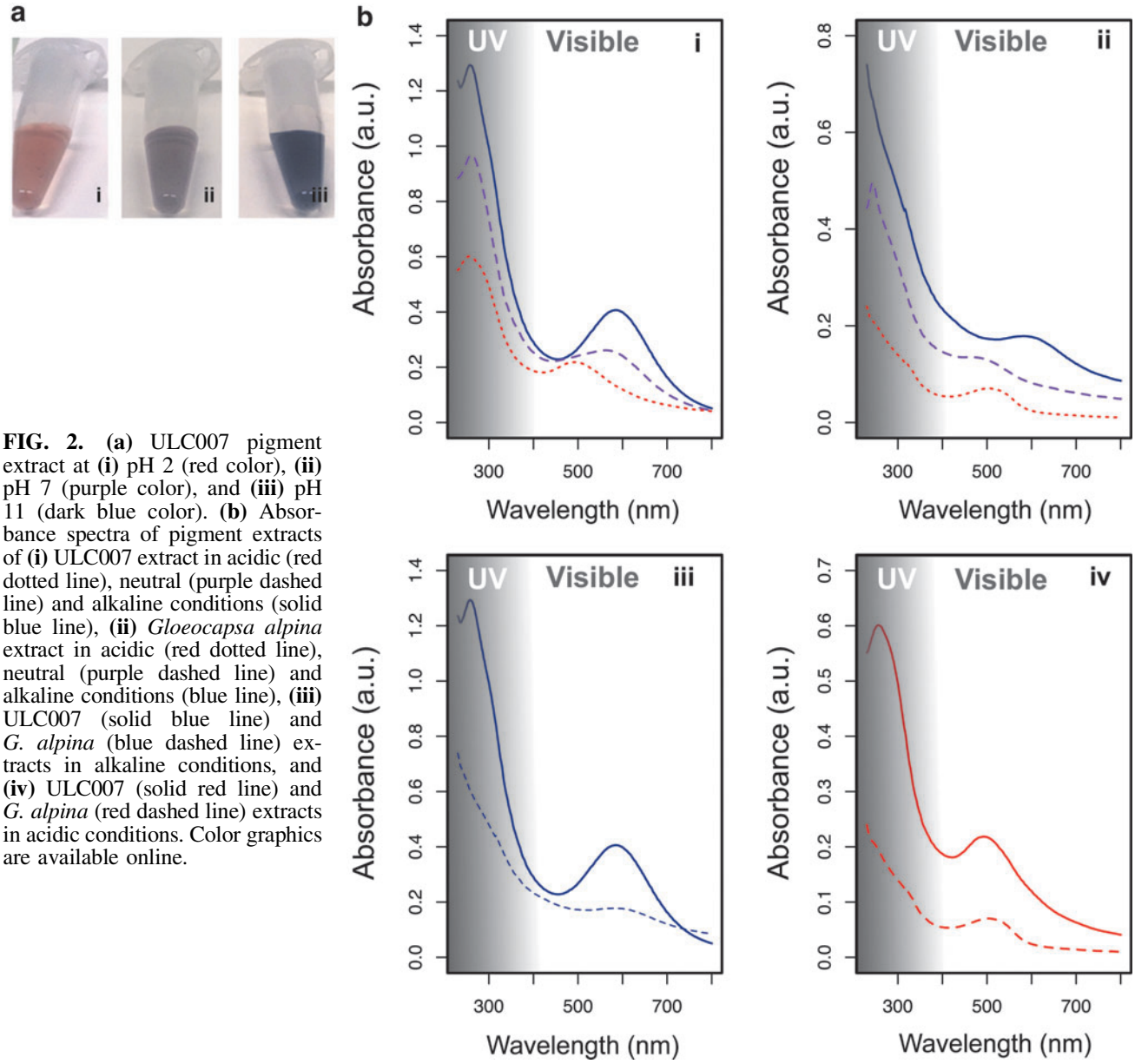

FIG. 2. **(a)** ULC007 pigment extract at **(i)** pH 2 (red color), **(ii)** pH 7 (purple color), and **(iii)** pH 11 (dark blue color). **(b)** Absorbance spectra of pigment extracts of **(i)** ULC007 extract in acidic (red dotted line), neutral (purple dashed line) and alkaline conditions (solid blue line), **(ii)** *Gloeocapsa alpina* extract in acidic (red dotted line), neutral (purple dashed line) and alkaline conditions (blue line), **(iii)** ULC007 (solid blue line) and *G. alpina* (blue dashed line) extracts in alkaline conditions, and **(iv)** ULC007 (solid red line) and *G. alpina* (red dashed line) extracts in acidic conditions. Color graphics are available online.

TABLE 1. MAXIMUM ABSORBANCES (λ MAX) OF GLOEOCAPSIN EXTRACTS IN ACIDIC AND ALKALINE CONDITIONS COMPARED TO OTHER MICROBIAL PIGMENTS

		λ max (nm)		
Pigment	*Color*	*UV wavelength*	*Visible wavelength*	*Reference*
Parietin	Yellow	225, 257, 265, 288	433	Manojlovic *et al.* (2010)
Emodin	Yellow	222, 253, 266, 289	436	Manojlovic *et al.* (2010)
Scytonemin	Yellow	252, 278, 300, 386		Proteau *et al.* (1993)
Scytonemin-3a-imine	Mahogany red	237, 366	437, 564	Grant and Louda (2013)
Putative gloeocapsin (ULC007)	Pink/red	256	492	This study
Putative gloeocapsin (ULC007)	Blue	258	585	This study

UV = ultraviolet.

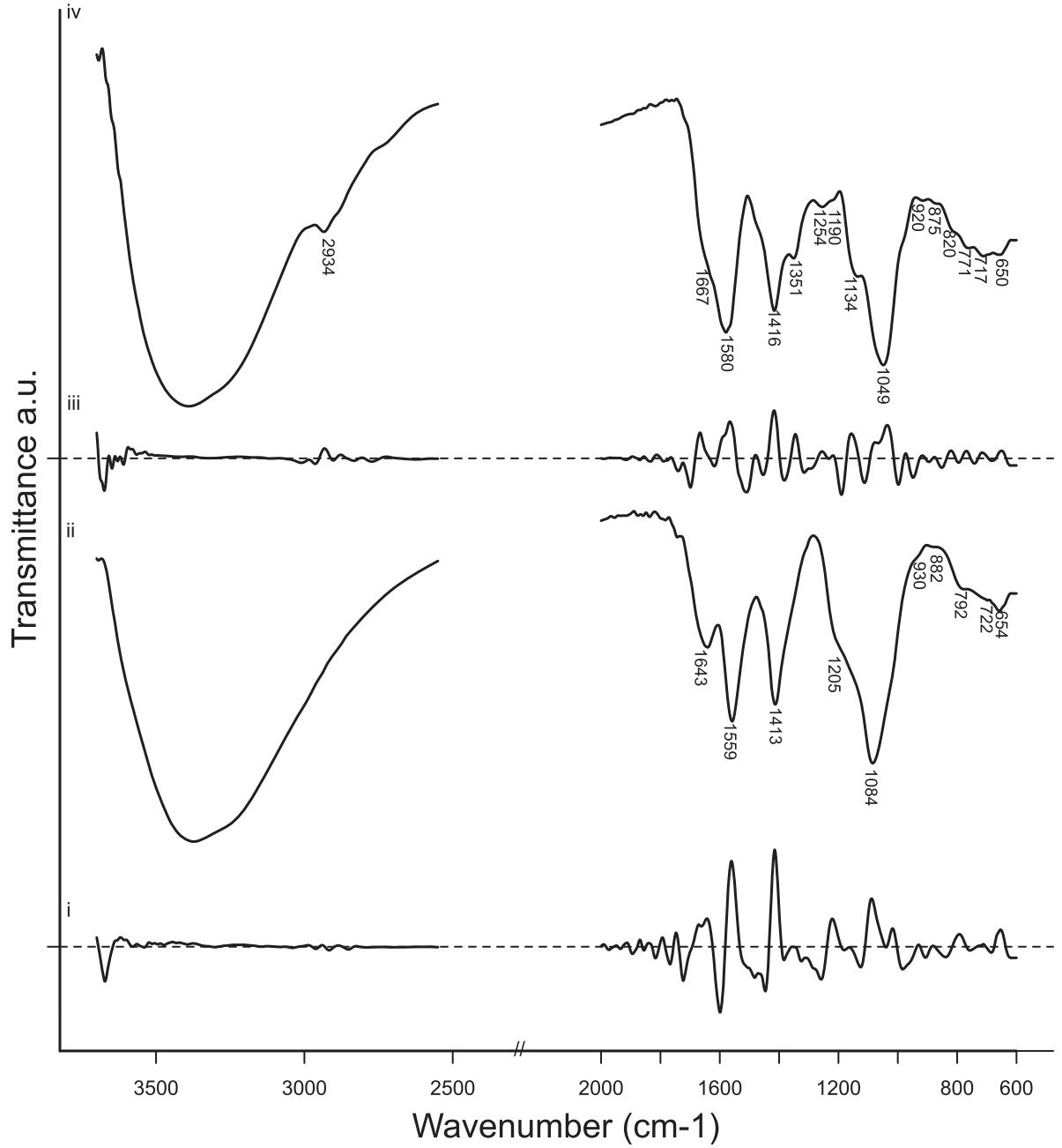

FIG. 3. Fourier-transform infrared spectrum and second derivative of **(i, ii)** ULC007 strain extracted pigment, and **(iii, iv)** *Gloeocapsa alpina* extract.

elongation. A very strong peak occurred at 1084 cm^{-1}, which may be due to the C–O stretch as already observed for carbohydrates such as glycogen (Wood *et al.*, 1998) or the phenolic group. The pigment extracted from the sample dominated by *Gloeocapsa* gave a rather similar FT-IR spectrum compared with one of the cultured strains.

Derivative curves confirmed the presence of shoulders at 1667 cm^{-1} for the *G. alpina* extract (C=C or C=O stretching) and 1205 cm^{-1} for the ULC007 extract (ring stretching).

To verify that the pigment was not altered by the extraction protocol, we first performed Raman mapping of a *G. alpina* colony from the environmental sample and of an empty sheath of *P. nigrescens* ULC007 before extraction (Fig. 4). Raman signatures of carotenoids and gloeocapsin were characterized by using R-HCA for *G. alpina* (Supplementary Fig. S2). The carotenoid signal was mainly detected inside the cells, whereas the gloeocapsin signal was detected in the EPS envelope. The gloeocapsin signal was more intense on the top left of the colony where the pigment seems to accumulate (Fig. 4i).

Bands assigned to gloeocapsin were 1672, 1588, 1464, 1360, 1320, 1292, 908, and 460 cm^{-1}. These bands were mixed with carotenoids bands 1516, 1156, and 1004 cm^{-1} (Fig. 4iii). For the empty sheath of *P. nigrescens* ULC007, the Raman signature of the gloeocapsin pigment was characterized by using the R-HCA approach (Supplementary Fig. S3). Bands assigned to gloeocapsin were 1675, 1575, 1480, 1435, 1385, 1325, 1280, 910, and 465 cm^{-1} (Fig. 4iii).

Table 2. FT-IR Vibrational Assignment for Gloeocapsins

Gloeocapsin						
Phormidesmis nigrescens ULC007	*Gloeocapsa alpina*	*Scytonemin*	*Scytonemin-3a-imine*	*Parietin*	*Approximate vibrational assignment*	
This study	*This study*	*Varnali* et al. *(2009)*	*Grant and Louda (2013)*	*Edwards* et al. *(2003)*	*Varnali* et al. *(2009)*	*Edwards* et al. *(2003)*
3700-2960	3700-2960	3431 3043 3020	3411.8	3413	ν(OH) ν(CH)aromatic ν(CH) vinylic	ν(OH)
	2934		2962 2922	2937		ν(CH3) assymmetric
				2845		ν(CH3) symmetric
		1714	1716		*ν*(C=O)	
				1675		ν(C=O) conjugated free
1643	1667	1652	1655		ν(C=C) conjugated *trans*	
				1630		ν(C=O) conjugated, H-bonded
		1628			ν(C=CH) attached to cyclopentene ring	
				1614		ν(C=C)aromatic; quadrant ring stretch
	1580	1589		1594	ν(CCH) aromatic ring quadrant stretch	ν(C = C) aromatic
1559				1569/1560		ν(C=C) aromatic
		1555		1478	ν(CCH) *p*-disubstituted aromatic ring	Ring stretch, coupled with OH
		1513	1451		ν(N = C-C = C) ring mode	
		1447		1452	δ(C = CH)	Ring strecth
1413	1416			1437		Ring strecth
		1385		1386	ν(CCN) indole ring	ν(C–O) phenyl
1348	1351		1376	1367	ν(CCN) indole ring	ν(C–O) phenyl
		1317		1325	ν(C = N) indole ring	Ring stretch, in plane
		1284			ν(CC) aromatic ring: p-disubstituted benzenes	
				1272		Ring stretch, in plane
1257	1254	1258		1256	ν(C = C—C = C) system (trans)	ν(C–O) aromatic ether
				1227		ν(C–O); d(OH) phenyl, in plane Ring stretch, C–C chelate
						Ring stretch, C–C chelate
1205				1200		Ring stretch, C–C chelate
	1190			1186		δ(OH) phenyl, free, in plane
		1173			ν(CC) ring breathing pyrrole	
	1134			1137		(C–CH) bend, in plane
		1110		1102	δ(COH) phenolic	(C–CH) bend, in plane
1084	1049	1091			ν(C-O) phenolic	

(*continued*)

TABLE 2. (CONTINUED)

Gloeocapsin						
Phormidesmis nigrescens ULC007	*Gloeocapsa alpina*	*Scytonemin*	*Scytonemin-3a-imine*	*Parietin*	*Approximate vibrational assignment*	
This study	*This study*	*Varnali* et al. *(2009)*	*Grant and Louda (2013)*	*Edwards* et al. *(2003)*	*Varnali* et al. *(2009)*	*Edwards* et al. *(2003)*
				1035		ν(C–O) aromatic ether
		1028		976	ν(C-O) phenolic	Ring breathing; δ(C–H) out of plane
930	920			926	δ(CNC)	δ(C–H) out of plane
882	875	877		901	δ(CCC)	
	820	840		874	δ(CCH) breathing disubstitueted aromatic ring	
				850		
792	771					
		755		757	δ(CCC/CCN) indole ring-puckering mode	ν(=C–H) aromatic, out-of-plane
722	717			715	δ(CCN) pyrrole ring-puckering mode	δ(OH) phenyl, out of plane
654	650					
				631		Skeletal deformation

Gloeocapsin signatures from both specimens were compared with spectra obtained for blue and red gloeocapsin observed by Storme *et al.* (2015) (Fig. 4iii).

Both extracts were further analyzed by Raman spectroscopy in acidic and alkaline pH conditions (Fig. 5 and Table 3). Raman bands assigned to gloeocapsin in the spectrum obtained for the extract of *G. alpina* and ULC007 under acidic conditions were observed at 1675/1677 cm^{-1} for ν(C=O) stretching, at 1565/1580 cm^{-1} for ν(C=C) stretching, at 1456/1479 cm^{-1} for δ(CH3) or δ(CH2), 1422/1441 cm^{-1} for ring stretching, 1179–1192 cm^{-1} for ν(C=C-C=C), and at 464 cm^{-1} for the aliphatic chain elongation.

Also, three strong bands were observed at 1363/1381, 1305/1323, and 1269/1281 cm^{-1}. These bands can be attributed to the breathing modes of heteroaromatic rings containing either nitrogen or oxygen (Table 3). While the band at 1305/1323 cm^{-1} may be assigned to the ν(C=N) of an indole ring as suggested by Edwards *et al.* (2005) and Jehlička *et al.* (2014) for the scytonemin, there is no evidence of the ν(C=C-C=N) ring mode at 1520 cm^{-1}. Also, the band located at 1281 cm^{-1} can be attributed to the amide III mode and might belong to proteins co-extracted from the sample together with the pigment.

However, the amide III mode cannot be observed without the amide II mode that is often more intense and located at 1550 cm^{-1}, which is not the case here. As shown in Fig. 5, similar Raman spectra were obtained for our two extracts and for *S. paulocellulare* previously described by Storme *et al.* (2015) under acid conditions. These similarities suggest a common molecular composition for all these samples, all of which seem to contain gloeocapsin. Only small differences are observed between the Raman spectra of the extracts in acidic conditions, which may be related to the occurrence of variant forms of gloeocapsin (different substituents) or to the co-extraction of other biomolecules during the extraction of both extracts.

In alkaline conditions, the Raman spectra obtained for both extracts are given in Fig. 5 and show fewer bands. The bands located at 1670 cm^{-1} for ν(C=O), at 1580 cm^{-1} for ν(C=C), and at 464 cm^{-1} for the aliphatic chain elongation are preserved. However, the bands located between 1200 and 1400 cm^{-1} are strongly affected, especially the band at ~1200 cm^{-1} attributed to the ring ν(C=C-C=C) elongation, which is not observed in the spectra obtained under alkaline conditions. In addition, the band around 1580 cm^{-1} appears broader in the spectra of both extracts under alkaline conditions. Therefore, changing from acidic to alkaline conditions of pH seems to strongly affect the structure of the aromatic cycles. A stronger band was observed at 1264 cm^{-1} for the environmental *G. alpina* sample extract, which could be attributed to the presence of more fatty acids in this extract (Movasaghi *et al.*, 2007).

The reverse HPLC chromatogram obtained for the *P. nigrescens* ULC007 extract under acidic conditions between 0 and 20 min is shown in Fig. 6. The eight most intense elution peaks (absorption at 256 nm) were investigated for the identification of the red pigment. Each peak corresponded to a unique eluted compound (**a–g**), listed in Table 4 with their putative molecular formula assignment. Fine isotopic profiles of the compounds of interest and their putative molecular formula are displayed in Supplementary Fig. S4.

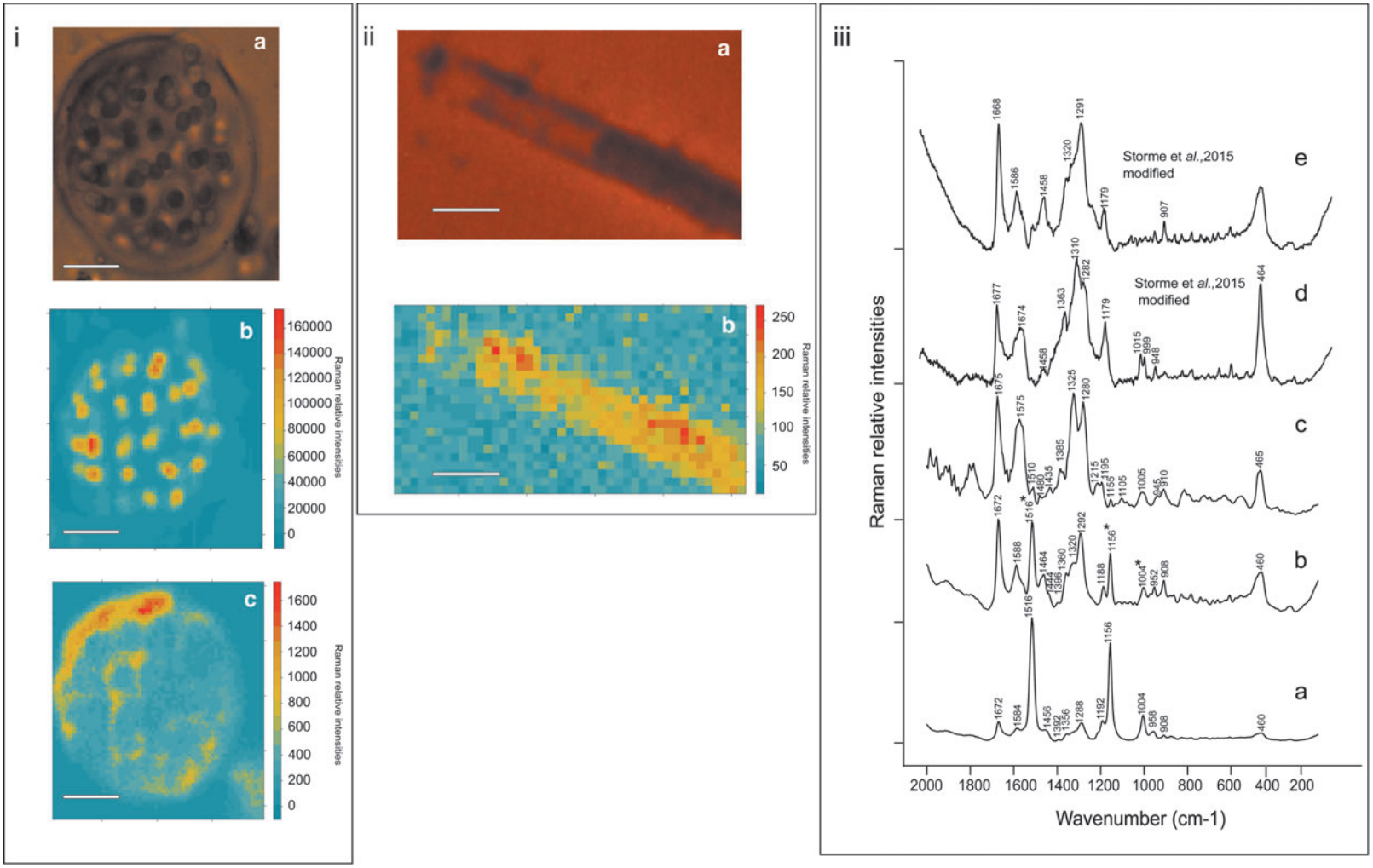

FIG. 4. Raman hyperspectral mapping of *Gloeocapsa alpina* and *Phormidesmis nigrescens* **(i-a)**, Picture of the *G. alpina* colony; **(i-b)**, Raman mapping of band intensities of carotenoids: δ3 (C-H) at 1004 cm^{-1}, v2 (C-C) at 1156 cm^{-1}, and v1 (C=C) at 1514 cm^{-1}; **(i-c)**, Raman mapping of the intensities of signature bands of gloeocapsin 460, 1292, 1320, and 1672 cm^{-1}; Scales represent 20 μm; **(ii-a)**, Picture of the empty EPS sheath of *P. nigrescens* ULC007; **(ii-b)**, Raman mapping of the intensities of signature bands of gloeocapsin 465, 1280, 1385, 1575, and 1675 cm^{-1}; **(iii)** Mean Raman spectra of cluster corresponding to **(a)** *G. alpina* cells, **(b)** extracellular pigment of *G. alpina* (gloeocapsin), **(c)** pigment in *P. nigrescens* ULC007 EPS sheath; **(d)** Raman spectra of blue gloeocapsin modified from Storme *et al.* (2015); **(e)** Raman spectra of red gloeocapsin modified from Storme *et al.* (2015). Color graphics are available online.

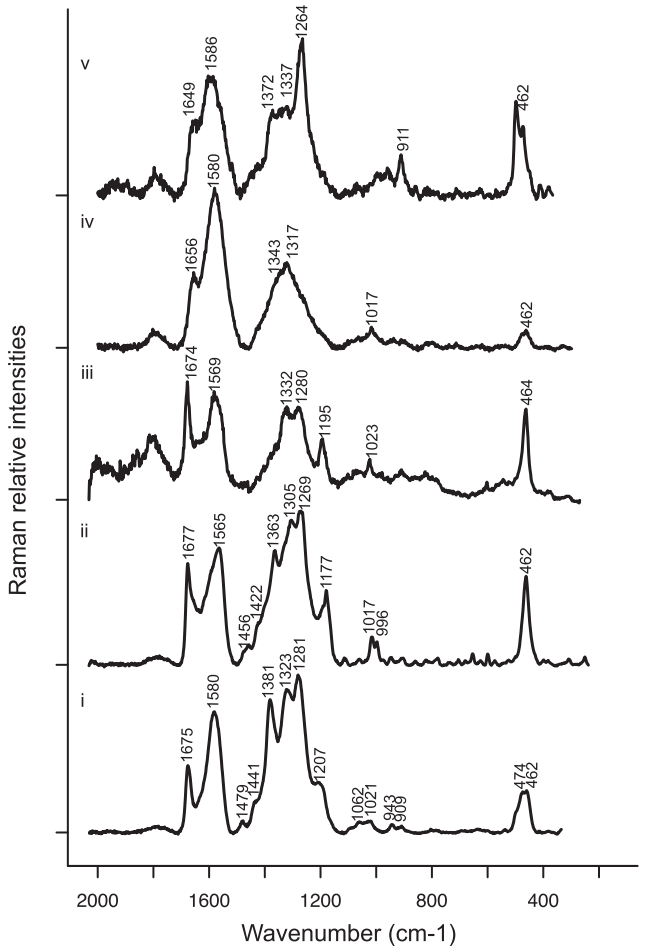

FIG. 5. Raman spectra in the **(i)** *Phormidesmis nigrescens* ULC007 extract in acidic conditions, **(ii)** the *Gloeocapsa alpina* extract in acidic conditions, **(iii)** *in situ Solentia paulocellulare* modified from Storme *et al.* (2015), **(iv)** *P. nigrescens* ULC007 extract in alkaline conditions, and **(v)** *G. alpina* extract in alkaline conditions.

The first eluting compound at a retention time (RT) of 9.1 min (compound **a**) was detected at *m/z* 355.049, and it corresponds to two molecular formulas: $C_{16}H_8N_4O_4$ or $C_{16}H_{12}O_8$. Both matching formulas show a high ring and double bond (rdb) value (16 and 11, respectively), which are expected for a compound absorbing the visible light. The compound **b** (341.0284 *m/z*), eluted at RT of 9.9 min and may correspond to either $C_{16}H_6N_4O_4$ or to $C_{17}H_8O_8$. The compound **c** (RT 10.28 min; 376.258 *m/z*) was identified as $C_{19}H_{35}N_3O_3$.

Even though this compound absorbs at 256 nm, it is unlikely to absorb in visible light as it has a low rdb number. The compound **d** at *m/z* 387.1915 and eluting at RT 11.2 min has three matching formulas ($C_{21}H_{26}N_2O_5$, $C_{24}H_{28}O_3$, and $C_{20}H_{24}N_6O$). This compound could be a potential chromophore, as rdb values for the three matching formulas were high (10, 11, and 12 respectively). The compound **e** is also a potential chromophore. It was detected at *m/z* 481.0745 (RT 12.20 min), and it has three potential matching molecular formulas $C_{17}H_{10}N_{14}O_2$, $C_{19}H_{22}O_{12}$, and $C_{22}H_{18}O_{11}$, which were also containing a relatively high rdb number (20, 9, and 14, respectively).

Since only $C_{19}H_{22}O_{12}$ and $C_{22}H_{18}O_{11}$ were matching existing compounds in the PubChem Database, the probability for $C_{17}H_{10}N_{14}O_2$ to be the correct formula assignment is low (Kim *et al.*, 2019). The compound **f** (RT 12.33 min; 433.0546 *m/z*) shows two possible matching molecular formulas: $C_{23}H_{12}O_9$ and $C_{21}H_{14}O_9$. With a rdb of 18 and 15, respectively, both formulas are likely to correspond to a chromophore. The compound **g** was detected at *m/z* 302.3042 eluting at 12.45 min, has been identified as $C_{18}H_{39}NO_2$, but shows no double bonds; this compound is, therefore, not corresponding to the targeted chromophore and will not be further analyzed. Finally, no matching compound formula has been found according to our molecular formula criteria for the *m/z* features detected at RT 17.78 min.

All the retained candidates (compounds **a**, **b**, **c**, **d**, **e**, and **f**) were searched against metabolites in CyanoMetDB, Metlin, and Norine databases (Caboche *et al.*, 2007; Guijas *et al.*, 2018; Jones *et al.*, 2021), however no matches with already described biomolecules were found in these databases. Fine isotopic profiles of the compounds of interest and their putatively corresponding molecular formula are displayed in Supplementary Information.

MS/MS spectra were used to bring additional information, thanks to fragmentation patterns and possibly discriminate candidate structures. The MS/MS spectra of compounds of interest detected in UV_{256nm} peaks a, b, c, d, e, and f are displayed in Fig. 7.

The product ion mass spectrum of compound **a** (Fig. 7i) showed neutral losses of CO and CH_2O, suggesting the presence of aldehydes, and neutral loss of CH_4O, suggesting the presence of a methyl ester function. From the obtained fragment, there is no evidence of the presence of nitrogen in the molecule. For the compound **b** MS/MS (Fig. 7ii) showed CO, CO_2, and H_2O neutral losses, which corresponded to a carboxylic acid function. The different fragments detected in the compound **c** product ion mass spectrum (Fig. 7iii) revealed the presence of a lipid chain ($C_4H_{10}O$ fragment detected) and of an amine function (HCN fragment detected).

The latter confirmed the presence of at least one nitrogen atom in its potential molecular formula. The MS/MS spectrum of compound **d** (Fig. 7iv) showed a neutral loss of CH_4O, potentially corresponding to a methyl ester function. Fragmentation of compound **e** (Fig. 7v) suggested the presence of either a carboxylic acid or an aldehyde function, and an isoprenyl function (C_4H_8). The fragmentation pattern of compound **f** (Fig. 7vi) shows a main fragment at *m/z* 390.0356, which has been identified as a CH_3CO loss, suggesting the presence of an ester group. The neutral loss of both H_2O and CO suggests the presence of at least one lactone ring in the molecule (Crotti *et al.*, 2004).

4. Discussion

4.1. Characterization of the pigment gloeocapsin

The production of a dark pigmented sheath by the strain ULC007 confirms that this strain belongs to the same clade as *P. nigrescens*, as suggested by Raabová *et al.* (2019). After extraction and partial purification, the colored extract still conserves its halochromic behavior. In addition, the comparison of the gloeocapsin Raman signature before and after extraction suggests that the chromophore and backbone

Table 3. Raman Approximate Vibrational Assignments for Gloeocapsin in Alkaline and Acidic Conditions

ULC007		*Gloeocapsin alpina*					
Acidic	*Alkaline*	*Acidic*	*Alkaline*	*Scytonemin*	*Parietin*	*Approximate vibrational assignment*	
This study	*This study*	*This study*	*This study*	*Varnali* et al. *(2009)*	*Edwards* et al. *(2003)*	*Varnali* et al. *(2009)*	*Edwards* et al. *(2003)*
514.5 nm	514.5 nm	514.5 nm	514.5 nm	1064 nm	1064 nm		
						ν(OH)	ν(OH)
					3069		
				3061	3036	ν(CH)aromatic	
				3028		ν(CH) vinylic	
							ν(CH3) assymmetric
					2919		
					2845		ν(CH3) symmetric
				1710		*ν*(C=O)	
1675		1677			1671		ν(C=O) conjugated free
	1656		1649	1652		ν(C=C) conjugated *trans*	
					1631		ν(C=O) conjugated, H-bonded
				1605		ν(C=CH) attached to cyclopentene ring	
					1613		ν(C=C)aromatic; quadrant ring stretch
1580	1580			1590	1594	ν(CCH) aromatic ring quadrant stretch	ν(C=C) aromatic
1565		1565			1553		ν(C=C) aromatic
			1550	1549	1479	ν(CCH) *p*-disubstituted aromatic ring	Ring stretch, coupled with OH
				1525		ν(N=C-C=C) ring mode	
1479		1456		1444	1449	δ(C=CH)	Ring strecth
1441		1422			1437		Ring strecth
1381				1384	1387	ν(CCN) indole ring	ν(C–O) phenyl
	1343	1363		1375	1370	ν(CCN) indole ring	ν(C–O) phenyl
1323	1317		1321	1323	1321	ν(C=N) indole ring	Ring stretch, in plane
		1305					
1281				1283		ν(CC) aromatic ring: p-disubstituted benzenes	
		1269	1264		1277		Ring stretch, in plane
				1245	1255	ν(C=C—C=C) system (trans)	ν(C–O) aromatic ether
1207					1216		Ring stretch, C–C chelate
					1198		Ring stretch, C–C chelate
					1180		Ring stretch, C–C chelate
		1177		1163	1160	ν(CC) ring breathing pyrrole	δ(OH) phenyl, free, in plane
					1137		(C–CH) bend, in plane
				1102	1104	δ(COH) phenolic	(C–CH) bend, in plane
1062				1090		ν(C-O) phenolic	
1021	1017	1017		1024	979	ν(C-O) phenolic	Ring breathing; δ(C–H) out of plane
943		966	911	984	926	δ(CNC)	δ(C–H) out of plane

(*continued*)

TABLE 3. (CONTINUED)

ULC007		*Gloeocapsin alpina*					
Acidic	*Alkaline*	*Acidic*	*Alkaline*	*Scytonemin*	*Parietin*	*Approximate vibrational assignment*	
This study	*This study*	*This study*	*This study*	*Varnali* et al. *(2009)*	*Edwards* et al. *(2003)*	*Varnali* et al. *(2009)*	*Edwards* et al. *(2003)*
				889	906	δ(CCC)	
				835		δ(CCH) breathing disubstitueted aromatic ring	
				754	765	δ(CCC/CCN) indole ring-puckering mode	ν(=C–H) aromatic, out-of-plane
				677	729	δ(CCN) pyrrole ring-puckering mode	δ(OH) phenyl, out of plane
					631		Skeletal deformation
					612		Skeletal deformation
				565	571	δ(CCN) aromatic ring indole system	Skeletal breathing
				539	519		
474				500		δ(CCCO) twist	
462	462	462	462		467		
					458		
				450		δ(NCCO) twist	

of the molecule is preserved after boiling and autoclaving. Spectral comparisons using UV-visible, Raman, and FT-IR spectroscopy confirm the spectral similarities between the pigment extracted from *P. nigrescens* ULC007 and the gloeocapsin observed in the environmental sample of Pont de Bonne that was dominated by *G. alpina*.

In previous studies, the chemical nature of the gloeocapsin was hypothetically related to either scytonemins (hypothesis 1), mainly because the latter are the only known dark extracellular UV-screening pigment present in cyanobacterial sheaths, or a class of molecules that contained anthraquinone (hypothesis 2), as previous spectroscopic analyses underlined similarities between parietin and gloeocapsin (Storme *et al.*, 2015).

However, in contrast to the previous UV-visible spectroscopic analyses of environmental *G. alpina* in acetone

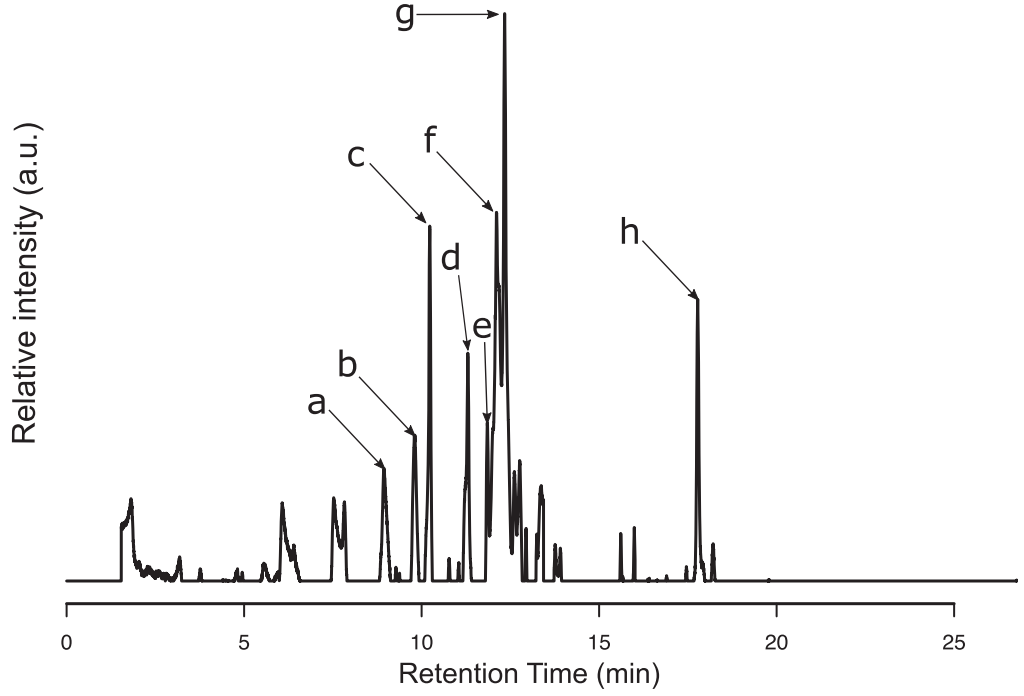

FIG. 6. RPLC UV_{256nm} chromatogram of *Phormidesmis nigrescens* ULC007 extract acidified. The arrows show the most intense UV_{256nm} peaks that were further investigated. UV = ultraviolet.

Table 4. Putative Molecular Formula Assignment of *m/z* Features Detected in the Most Intense $UV_{256\ nm}$ Peaks (a to g)

Detected m/z	*Peak*	*Retention time*	*Neutral molecular formula*	*Error (ppm)*	*mSigma*	*rdb*	*Adduct*	*O/C*	*N/C*	*H/C*
355.0429	a	9.1	$C_{17}H_8N_4O_4$	2.5	16.3	16	Na	0.235	0.235	0.471
355.0429	a	9.1	$C_{16}H_{12}O_8$	−1.2	25.1	11	Na	0.5	0	0.750
341.0284	b	9.9	$C_{16}H_6N_4O_4$	−0.7	14.8	16	Na	0.250	0.250	0.375
341.0284	b	9.9	$C_{17}H_8O_8$	2.4	19.4	14	H	0.471	0	0.471
376.258	c	10.28	$C_{19}H_{35}N_3O_3$	−2.4	9.2	4	Na	0.158	0.158	1.842
387.1915	d	11.2	$C_{21}H_{26}N_2O_5$	−0.2	37.6	10	H	0.238	0.095	1.286
387.1915	d	11.2	$C_{24}H_{28}O_3$	4	46.3	11	Na	0.125	0	1.167
387.1915	d	11.2	$C_{20}H_{24}N_6O$	−2.9	41.3	12	Na	0.050	0.3	1.200
481.0745	e	12.20	$C_{17}H_{10}N_{14}O_2$	−0.5	23.4	20	K	0.118	0.823	0.558
481.0745	e	12.20	$C_{19}H_{22}O_{12}$	−0.2	28.7	9	K	0.632	0	1.158
481.0745	e	12.20	$C_{22}H_{18}O_{11}$	−0.8	15.5	14	Na	0.5	0	0.818
433.0546	f	12.33	$C_{23}H_{12}O_9$	1.9	12.7	18	H	0.391	0	0.527
433.0546	f	12.33	$C_{21}H_{14}O_9$	−3.7	15.2	15	Na	0.429	0	0.667
302.3042	g	12.45	$C_{18}H_{39}NO_2$	3.9	4.4	0	H	0.111	0.056	2.167

mSigma is corresponding to the isotopic pattern fit factor. A low mSigma value corresponds to a high isotopic profile fit. Rdb corresponds to the number of rings and double bounds in the molecular formula.
rdb = ring and double bond.

(Storme *et al.*, 2015), we did not observe any peaks that could be related to chlorophylls or other known pigment in our study. Indeed, the NaOH treatment followed by several washings of the pellet in polar organic solvent appeared to be efficient enough to remove the photosynthetic pigments. Our UV-visible absorbance spectra exhibited more than one maximum, which is also the case for scytonemins (Grant and Louda, 2013) or quinoids (Manojlovic *et al.*, 2010). The first maximum of absorption in the UV region mainly covered the UVC and UVB wavelengths.

In acidic conditions (λ_{max}: 256, 492 nm *in vitro*), the UV-visible spectrum of the ULC007 extract is comparable to the one observed for the red scytonemin-3a-imine (λ_{max}: 237, 366, 437, 564 nm *in vitro*) by Grant and Louda (2013). However, multiple maxima often occur in the case of microbial UV-screening pigments.

The second absorption maximum in the visible region corresponds to the halochromism of the gloeocapsin. More precisely, we suggest that (de)protonation of gloeocapsin chromophores affected its absorption in the visible range and is likely to be responsible for the halochromism effect. In this case, the pigment would comprise molecular functions that are sensitive to (de)protonation, which might lead to the reversible oxidation and reduction of the molecule depending on the pH. In consequence, the ''purple'' color of the solution at intermediate or neutral pH would result from the presence of the two forms of the molecule. (De)Protonation can also occur in the case of scytonemins. For instance, the scytonemin-3a-imine is also altered by the addition of a reducing agent to C=O instead of the alcohol functions (Grant and Louda, 2013). However, in this case, (de)protonation does not provoke a shift of color.

Both acidic and alkaline extracts absorb in the UV range of wavelengths. Nevertheless, the actual UV-screening efficacy of the molecule remains to be proven, for example by induction of its production after UV irradiation, or by measuring the protection against UV damage in DNA (Cockell and Knowland, 1999).

The FT-IR spectra of the Pont de Bonne sample (*G. alpina*) and of strain ULC007 (*P. nigrescens*) also strongly suggest a common backbone structure of the pigments present in both extracts. More precisely, IR spectroscopy evidences the presence of aromatic compounds, consistent with the high absorbance observed in the UV wavelengths, and as can be observed for benzene (Cockell and Knowland, 1999). The IR analyses did not allow us to clearly confirm the presence of nitrogen in the targeted chromophore, as nitrogen-containing groups such as imine and azo groups exhibit absorption close to alkene and carbonyl double stretching regions (Coates, 2006).

Raman spectra of Pont de Bonne *G. alpina* and *P. nigrescens* ULC007 extracts in acidic conditions are congruent with the previous *in situ* Raman spectroscopic analyses for the two lineages *G. alpina* and *S. paulocellulare* (Storme *et al.*, 2015). The comparison of Raman spectra of the three lineages (*G. alpina*, *P. nigrescens* ULC007, *S. paulocellulare*), as shown by Fig. 4, confirms that their pigments potentially share a common structure and belong to the same class of compounds: the gloeocapsins. Interestingly, as previously observed, gloeocapsins share a few vibration frequencies with scytonemin (hypothesis 1) and more with parietin (hypothesis 2) (Storme *et al.,* 2015), but these vibration frequencies are common for N-heteroaromatic compounds and can also be found in other molecules such as coumarin (Vogel and Kiefer, 1998), quercitin, and other flavonoids (Numata and Tanaka, 2011; Pompeu *et al.*, 2018). Therefore, the presence of these equivocal bands does not allow to classify gloeocapsins as scytonemins nor as anthraquinones.

The HPLC-UV-MS/MS analysis of the extract of *P. nigrescens* ULC007 non-axenic culture allows the detection of five compounds that may potentially correspond to gloeocapsin. Based on the Raman spectra, the gloeocapsin molecule should contain at least one unsaturation [peak at 1667 cm^{-1} for a ν(C=C) stretching vibration] and one oxygen atom [1084 cm^{-1} peak for either a ν(C-O) stretch or a

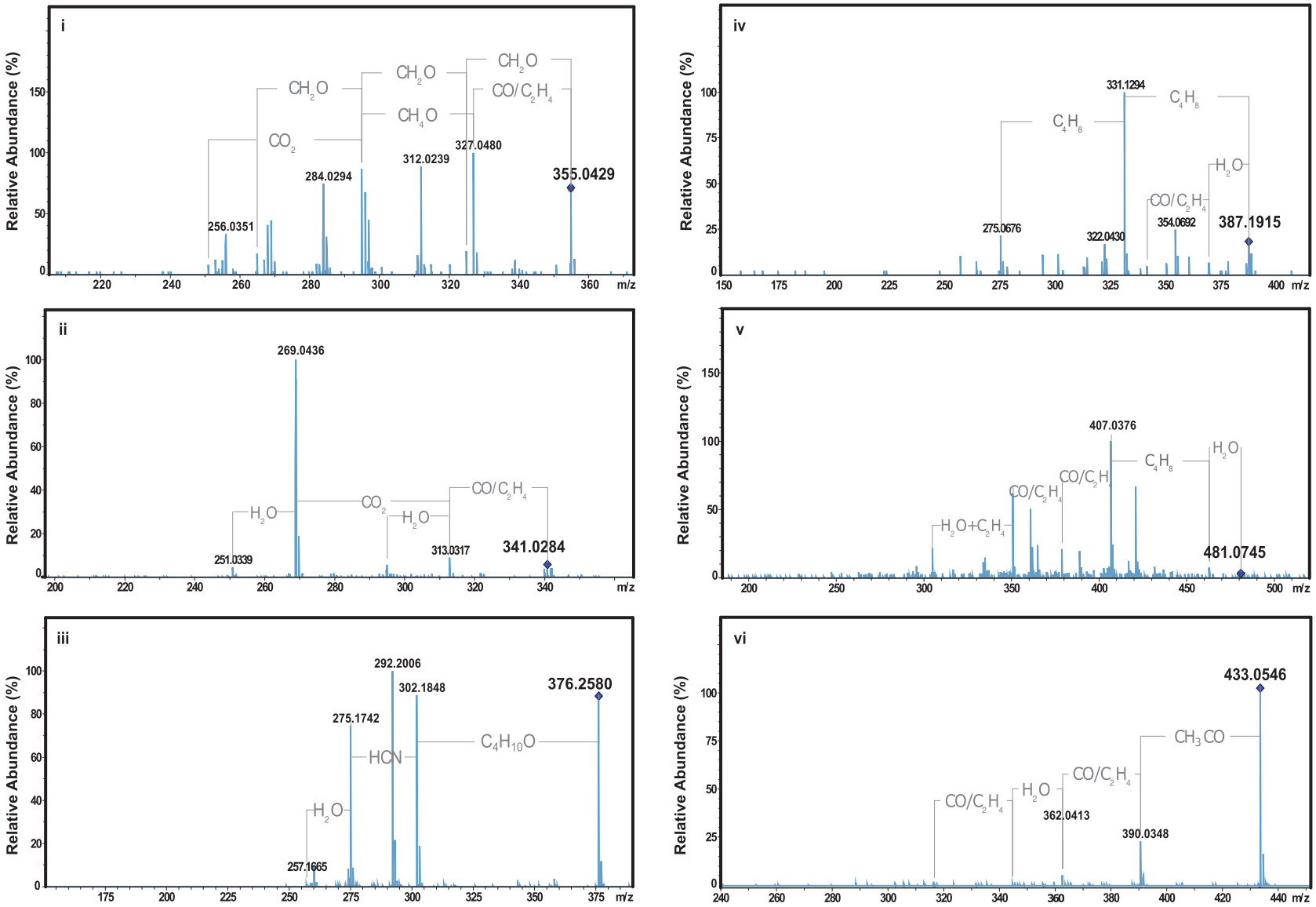

FIG. 7. Product ion mass spectra of **(i)** *m/z* 355.0429, **(ii)** *m/z* 341.0284, **(iii)** *m/z* 376.2580, **(iv)** *m/z* 387.1915, **(v)** *m/z* 481.0742, and **(vi)** *m/z* 433.0546. Color graphics are available online.

phenolic compound]. All gloeocapsin candidates show some functional groups containing oxygen. In contrast, none of the MS/MS fragments could confirm the presence of nitrogen atoms, rejecting the hypothesis (1) that gloeocapsins would be related to scytonemins.

Interestingly, the PubChem results for the assigned molecular formula, without nitrogen, match anthraquinone derivatives (compound **b**: $C_{17}H_8O_8$ and compound **d**: $C_{21}H_{14}O_9$), coumarin derivatives (compound **f**: $C_{23}H_{12}O_9$), and quercetin derivatives (compound **a**: $C_{16}H_{12}O_8$) or other flavonoid derivatives (compound **e**: $C_{22}H_{18}O_{11}$), commonly found in cyanobacteria (Singh *et al.*, 2017; Demay *et al.*, 2019; Żyszka-Haberecht *et al.*, 2019). However, the previous observations by Storme *et al.* (2015), which favored the second (parietin) hypothesis, relied on spectroscopic data obtained from a sample dominated by epilithic *Gloeocapsa*-like colonies on gypsum and possibly wrongly attributed to parietin (Edwards *et al.*, 2005).

Indeed, the attribution of vibrational bands to parietin was discussed for six Raman bands, which are not exclusive to parietin as they can also be observed for other pigments or halochromic compounds such as flavonoids (Pompeu *et al.*, 2018). Moreover, parietin is known to be produced only by lichens of the Teloschistales order and is found in the roots of the plant *Rumex crispus* (Choi *et al.*, 2004), but it has never been found in free-living (non symbiotic) cyanobacterial cells, except for the report in the study of Edwards *et al.* (2005).

In contrast, gloeocapsin was previously reported in the lichen *E. granatina*, which has two photobionts that include *Gloeocapsa sanguinea* (Büdel and Henssen, 1988). Therefore, it is likely that Edwards *et al.* (2005) were reporting the detection of gloeocapsin back in 2005 instead of parietin.

Our study permits to propose a third hypothesis (3), where the gloeocapsin belongs to another class of compounds capable of halochromism such as the coumarins, or flavonoids.

Although the precise chemical formula and structure of gloeocapsin still remain to be elucidated, the RTs and masses acquired during this study permitted to narrow down its chemical composition to potentially five candidates within three classes of halochromic molecules: anthraquinone derivatives, coumarin derivatives, and flavonoids. This will sustain further studies to test the hypotheses (2) and (3) and ascertain the definite structure of gloeocapsin, and it will also require the optimization of culture growth and pigment production to obtain the substantial biomass needed to perform preparative chromatography, beyond the scope of this study.

So far, no homolog of the scytonemin gene cluster (*scy*) was found in two independent annotated assemblies of ULC007 available in the GenBank database (Lara *et al.*, 2017; Moore *et al.*, 2019). However, other gene clusters known to be responsible for secondary metabolites were found in the genome sequence of ULC007 (Lara *et al.*, 2017). One of them, a type 2 polyketide synthase PKS-like gene cluster could be involved in the biosynthesis of an anthraquinone derivative as is the case for the gammaproteobacterium *Photorabdus luminescens* (Brachmann *et al.*, 2007).

Other secondary metabolite biosynthetic gene clusters responsible for the production of molecules that contain aromatic compounds such as quinoid without amide functions could also be investigated as they are also found in bacteria and are widespread in the cyanobacterial phylum (Sivonen *et al.*, 2010; Cimermancic *et al.*, 2014). Depending on the elucidation of the gloeocapsin structure, it should be possible to find candidate genes among those described earlier and present in ULC007 to characterize the biosynthetic pathway of this halochromic pigment.

4.2. Implications for the evolution of phototrophy and astrobiology

The wide distribution of gloeocapsin-producing strains among the cyanobacterial phylum in three distinct orders (Chroococcales, Pleurocapsales and Synechococcales) suggests its occurrence in a common ancestor. Nevertheless, despite the large diversity of their present-day habitats (freshwater Antarctic mat, marine euendolith, continental freshwater epilith), early lateral gene transfer events cannot yet be excluded without extensive genomic studies. These hypotheses should be tested in the future with appropriate genetic analyses.

Occurrence in a common ancestor implies the early invention of this biosynthetic pathway, and of its extracellular secretion mechanism. On the Early Earth, cyanobacteria and their ancestors must have evolved under harsh surface conditions during the Precambrian. Unambiguous fossil cyanobacteria are 1.9 Ga old (Hofmann, 1976; Knoll and Golubic, 1992; Butterfield, 2015; Demoulin *et al.*, 2019; Javaux, 2019). Oxygenic photosynthesis impacted Earth ocean and atmosphere at a planetary scale by at least 2.4 Ga (the age of the Great Oxidation Event [GOE]), but paleoredox proxies suggest two possible AOE (mild Archean Oxygenation Events) at 2.5 and 2.65 Ga, and older more ambiguous low-oxidation events, before the GOE (Ostrander *et al.*, 2021); and recent molecular phylogenies of oxygen-dependent enzymes also suggest the availability of oxygen before the GOE, around 3.1 Ga (Jabłońska and Tawfik, 2021).

The lack of an ozone layer is, however, indicated by mass-independent fractionation of sulfur isotopes before the GOE (Farquhar *et al.*, 2005). These conditions probably drove the emergence of adaptations at the genomic and metabolic levels that seem to persist in modern cyanobacteria. Ancestral cyanobacteria may have been exposed to high doses of both UVC (>280 nm) and UVB (280–350 nm) radiations (Cockell, 1998; Garcia-Pichel, 1998; Golubic and Abed, 2010; Garcia-Pichel *et al.*, 2019), due to the lack of O_3 in the atmosphere (Jackson, 2015).

Such radiations are known to provoke irreversible effects in cells by directly damaging nucleic acids, proteins, and lipids, or by creating reactive oxygen species (ROS). Besides, UV radiations also inhibit photosynthesis by damaging the D1/D2 proteins in the reaction center of the photosystem II. In such conditions, ancestral cyanobacteria, if already present, would need to develop original strategies to protect their photosystems and cellular integrity (*e.g.*, motility, ROS-binding enzymes, fast DNA repair mechanisms, UV-absorbing molecules) (Wynn-Williams *et al.*, 2002; Castenholz and Garcia-Pichel, 2012).

Among these strategies, the biosynthesis of photoprotective pigments, which may also be ROS-protective molecules such as polyphenols (coumarins, flavonoids), may

have enabled cyanobacteria and other phototrophic bacteria to colonize shallow waters and terrestrial habitats before 2.4 Ga (Jackson, 2015), perhaps as early as 3.2 Ga (Homann *et al.*, 2018). The UV-screening pigments were, thus, probably very instrumental for the colonization of exposed surface habitats on the early Earth that might have happened in parallel to the adaptation to cryptic endolithic niches.

Several microfossils interpreted as possible cyanobacteria exhibit extracellular envelopes with darker layers, possibly due to the presence of pigments (Golubic and Hofmann, 1976; Storme *et al.*, 2015). The best-known example is the oldest unambiguous cyanobacterial microfossil *Eoentophysalis belcherensis* ($\sim$1.9 Ga), which displays an extracellular envelope around the colonies with darker cells concentrated at the surface. Other microfossils such as *Eogloeocapsa*, *Gloeodiniopsis*, and *Polybessurus* have possible modern analogues (*Gloeocapsa* spp. and *Solentia* spp.) that produce gloeocapsin and also display multilayered envelopes with dispersed organic matter (Sergeev *et al.*, 2012; Demoulin *et al.*, 2019; Ouyang *et al.*, 2021).

As scytonemin and gloeocapsin are exclusively produced by cyanobacteria, their presence or traces in the fossil record would be a robust criterion to unambiguously identify a microfossil as a cyanobacterium. Moreover, *P. nigrescens* ULC007 studied here looks very similar to small filamentous microfossils that are abundant in the Precambrian rock record and have been interpreted as possible cyanobacteria (i.e., *Siphonophycus* and *Gunflintia*). In this case, if the presence of gloeocapsin (or its diagenetic derivative) could be demonstrated, it would be a convincing criterion to reassess the evolutionary affinity of these microfossils with a very simple morphology.

Although our case study applies to specific pigments produced by complex Earth microorganisms (cyanobacteria), the data presented in this article may provide general insights into the types of molecular structures indicative of UV-screening strategy, which could perhaps be sought beyond Earth. Starlight is a source both of strong lethal radiations (*e.g.*, UV) and of an unlimited and efficient energy. Therefore, life on Earth has developed strategies to protect itself from the harmful radiations and at the same time, to use photons from the visible to infrared wavelengths (*i.e.*, phototrophy) very early on (more than 3.4 Ga). If life exists elsewhere, it might have evolved analogous strategies.

However, much work remains to be done to understand and characterize the diversity of abiotic processes and their products forming pseudosignatures of life (abiotic organic and/or mineral structures, molecules or patterns resembling life) on the early Earth, early Mars, and beyond (Javaux, 2019; García-Ruiz *et al.*, 2020; McMahon and Cosmidis, 2021). In the case of pigments, since complex organic compounds such as pyrroles and porphyrins (chlorophyll and hemes building blocks) can form abiotically (Simionescu *et al.*, 1978; Fox and Strasdeit, 2013), their biogenicity is only supported when they are closely associated with morphological traces of life, such as filamentous sheaths, colonial envelopes, cell walls, and microbial mats, formed and preserved in a geological context that can exclude any possible abiotic origin of such possible molecular and morphological biosignatures.

The building blocks of other pigments such as *all-trans* retinal and carotenoids (polyene structure and aromatic ring), scytonemin (tryptophan), and gloeocapsin (polyphenols and polycyclic aromatic carbon compounds) are known to form abiotically (McCollom and Simoneit, 1999; Kwok, 2017; Ménez *et al.*, 2018; d'Ischia *et al.*, 2021). Therefore, complex organic molecules similar to pigments may perhaps provide robust biosignatures only when preserved in close association with other morphological and chemical traces of life, in a relevant photic habitable and preservation context that can exclude an abiotic origin.

5. Conclusion

In this work, we report and characterize the spectroscopic features useful for the characterization of the halochromic and UV-screening pigment gloeocapsin exclusively produced by cyanobacteria, and we investigate potential masses and formulas consistent with the chemistry of this enigmatic pigment.

The combination of several analytical approaches in this study revealed that gloeocapsin is a pigment distinct from the previously known scytonemin and unique to cyanobacteria.

The chemical nature of gloeocapsin has long been questioned. Here, we confirm that this pigment differs from known molecules, and we propose five candidate compounds for future analysis and definitive elucidation of the gloeocapsin structure. We also highlight evidence suggesting that gloeocapsin occurs in at least three clades and thus is potentially widespread within the phylum of cyanobacteria, and it may have possibly been produced by a common ancestor, as an early adaptation to early Earth harsh surface conditions.

In addition to contributing to the fundamental biological knowledge of these important primary producers and plastid ancestors, our study also provides a new molecular biosignature: gloecocapsin. The detection of this taxonomically informative pigment, in addition to the previously known scytonemin, could permit the identification of ambiguous microfossils as cyanobacteria in the early rock record and help reconstruct their evolution in Precambrian ecosystems.

The spectroscopic signatures obtained during this study will also be useful for referencing the presence of gloeocapsin in biological, ecological, and geological studies. Because star light is an efficient and abundant source of energy, it is possible that extraterrestrial life, if it exists, may have developed phototrophy, using pigments to harvest photons and to protect against UV radiations. Therefore, the combination of preserved morphologies (sheath, mats) and complex organic molecules involved in phototrophy and UV-screening might be an interesting target for astrobiological search for life in extraterrestrial ancient sediments, such as during the NASA Perseverance mission, the ESA-ROSCOSMOS ExoMars 2022, both equipped with imaging and spectroscopic instruments, and also with mass spectrometry in the case of the ExoMars Rover Rosalind Franklin, and in future Mars samples returned to Earth.

Author Disclosure Statement

No competing financial interests exist.

Funding Information

Research funding came from the European Research Council StG ELiTE (FP7/308074), the BELSPO IAP

PLANET TOPERS, the FRS-FNRS-FWO EOS ET-HoME (EOS30442502) and Rhizoclip (EOS30650350) projects, ULiege mini-ARC PUMA project, BELSPO projects CCAMBIO (SD/BA/03), and BRAIN 2.0 PORTAL (B2/212/P1/PORTAL). Annick Wilmotte is Senior Research Associate of the FRS-FNRS.

Supplementary Material

Supplementary Table S1
Supplementary Figure S2
Supplementary Figure S3
Supplementary Figure S4

References

Beleites C and Sergo V (2021). *hyperSpec: a package to handle hyperspectral data sets in R. R package version 0.100.0*. Available online at https://github.com/r-hyperspec/hyperSpec

Biondi N, Tredici MR, Taton A, *et al*. (2008) Cyanobacteria from benthic mats of Antarctic lakes as a source of new bioactivities. *J Appl Microbiol* 105:105–115.

Blumenberg M, Thiel V, and Reitner J (2015) Organic matter preservation in the carbonate matrix of a recent microbial mat—is there a 'mat seal effect'? *Org Geochem* 87:25–34.

Bonifacio A, Beleites C, and Sergo V (2015) Application of R-mode analysis to Raman maps: a different way of looking at vibrational hyperspectral data. *Analy Bioanal Chem* 407: 1089–1095.

Brachmann AO, Joyce SA, Jenke-Kodama H, *et al*. (2007) A type II polyketide synthase is responsible for anthraquinone biosynthesis in *Photorhabdus luminescens*. *ChemBioChem* 8: 1721–1728.

Brocks JJ, Love GD, Summons RE, *et al*. (2005) Biomarker evidence for green and purple sulphur bacteria in a stratified Palaeoproterozoic sea. *Nature* 437:866–870.

Büdel B and Henssen A (1988) *Trebouxia aggregata* und *Gloeocapsa sanguinea*, Phycobionten in *Euopsis granatina* (Lichinaceae). *Plant Syst Evol* 158:235–241.

Butterfield NJ (2015) Proterozoic photosynthesis—a critical review. *Palaeontology* 58:953–972.

Caboche S, Pupin M, Leclere V, *et al*. (2007) NORINE: a database of nonribosomal peptides. *Nucleic Acids Res* 36: D326–D331.

Castenholz RW and Garcia-Pichel F (2012) Cyanobacterial responses to UV radiation. In *Ecology of Cyanobacteria II*, edited by B.A. Whitton, Springer, Dordrecht, pp 481–499.

Choi GJ, Lee S-W, Jang KS, *et al*. (2004) Effects of chrysophanol, parietin, and nepodin of *Rumex crispus* on barley and cucumber powdery mildews. *Crop Prot* 23:1215–1221.

Cimermancic P, Medema MH, Claesen J, *et al*. (2014) Insights into secondary metabolism from a global analysis of prokaryotic biosynthetic gene clusters. *Cell* 158:412–421.

Coates J (2006) Interpretation of infrared spectra, a practical approach. In *Encyclopedia of AnalyticalChemistry Book series*, edited by R.A. Meyers and M.L. McKelvy, John Wiley & Sons, Hoboken, USA.

Cockell CS (1998) Biological effects of high ultraviolet radiation on early earth—a theoretical evaluation. *J Theor Biol* 193:717–729.

Cockell CS and Knowland J (1999) Ultraviolet radiation screening compounds. *Biol Rev* 74:311–345.

Crotti AEM, Fonseca T, Hong H, *et al*. (2004) The fragmentation mechanism of five-membered lactones by electrospray ionisation tandem mass spectrometry. *Int J Mass Spectrom* 232:271–276.

Demay J, Bernard C, Reinhardt A, *et al*. (2019) Natural products from cyanobacteria: focus on beneficial activities. *Mar Drugs* 17:1–49.

Demoulin CF, Lara YJ, Cornet L, *et al*. (2019) Cyanobacteria evolution: insight from the fossil record. *Free Radic Biol Med* 140:206–223.

d'Ischia M, Manini P, Martins Z, *et al.* (2021) Insoluble organic matter in chondrites: Archetypal melanin-like PAH-based multifunctionality at the origin of life? *Phys Life Rev* 37:65–93.

Edwards HGM, Newton EM, Wynn-Williams DD, *et al*. (2003) Molecular spectroscopic studies of lichen substances 1: parietin and emodin. *J Mol Struct* 648:49–59.

Edwards HGM, Villar SEJ, Parnell J, *et al*. (2005) Raman spectroscopic analysis of cyanobacterial gypsum halotrophs and relevance for sulfate deposits on Mars. *Analyst* 130:917–923.

Farquhar J, Jackson TL, and Thiemens MH (2000) A 33S enrichment in ureilite meteorites: evidence for a nebular sulfur component. *Geochim Cosmochim Acta* 64:1819–1825.

Fox S and Strasdeit H (2013) A possible prebiotic origin on volcanic islands of oligopyrrole-type photopigments and electron transfer cofactors. *Astrobiology* 13:6 578–595.

Gademann K and Portmann C (2008) Secondary metabolites from cyanobacteria: complex structures and powerful bioactivities. *Curr Org Chem* 12:326–341.

Garcia-Pichel F (1998) Solar ultraviolet and the evolutionary history of cyanobacteria. *Orig Life Evol Biosph* 28:321–347.

Garcia-Pichel F and Castenholz RW (1991) Characterizaton and biological implications of scytonemin, a cyanobacterial sheat pigment. *J Phycol* 27:395–409.

Garcia-Pichel F, Wingard CE, and Castenholz RW (1993) Evidence regarding the ultraviolett sunscreen role of the Mycosporin-like compounds in the cyanobacterium *Gloeocapsa* sp. *Appl Environ Microbiol* 59:170–176.

Garcia-Pichel F, Lombard J, Soule T, *et al*. (2019) Timing the evolutionary advent of cyanobacteria and the later great oxidation event using gene phylogenies of a sunscreen. *MBio* 10:1–14.

García-Ruiz JM, van Zuilen MA, and Bach W (2020) Mineral self-organization on a lifeless planet. *Phys Life Rev* 34–35 62–82.

Golubic S and Abed RMM (2010) *Entophysalis* mats as environmental regulators. In *Microbial Mats: Modern and Ancient Microorganisms in Stratified Systems*, edited by J. Seckbach and A. Oren, Springer, Netherlands, pp 237–251.

Golubic S and Hofmann HJ (1976) Comparison of holocene and mid-precambrian Entophysalidaceae (Cyanophyta) in stromatolitic algal mats: cell division and degradation. *J Paleontol* 50:1074–1082.

Grant CS and Louda JW (2013) Scytonemin-imine, a mahogany-colored UV/Vis sunscreen of cyanobacteria exposed to intense solar radiation. *Org Geochem* 65 29–36.

Gueneli N, Mckenna AM, Ohkouchi N, *et al*. (2018) 1.1-billion-year-old Porphyrins establish a marine ecosystem dominated by bacterial primary producers. *Proc Natl Acad Sci U S A* 115:E6978–E6986.

Guijas C, Montenegro-Burke JR, Domingo-Almenara X, *et al*. (2018) METLIN: a technology platform for identifying knowns and unknowns. *Anal Chem* 90:3156–3164.

Hirschberg J and Chamovitz D (1994) Carotenoids in cyanobacteria. In *The Molecular Biology of Cyanobacteria*, edited by D.A. Bryant. Springer, Dordrecht, pp 559–579.

Hodgson DA, Verleyen E, Squier AH, *et al*. (2006) Interglacial environments of coastal east Antarctica: Comparison of MIS

1 (Holocene) and MIS 5e (Last Interglacial) lake-sediment records. *Quat Sci Rev* 25:179–197.

Hofmann HJ (1976) Precambrian microflora, Belcher Islands, Canada: significance and systematics. *Jf Paleontol* 50:1040–1073.

Homann M, Sansjofre P, Van Zuilen M, *et al*. (2018) Microbial life and biogeochemical cycling on land 3,220 million years ago. *Nat Geosci* 11:665–671.

Jaag O (1945) Untersuchungen über di Vegetation und Biologie der Algen des nackten Gesteins in den Alpen, im Jura und im schweizerischen Mittelland. *Beiträge zur Kryptogamenflora der Schweiz* 9:1–560.

Jabłońska J and Tawfik DS (2021) The evolution of oxygen-utilizing enzymes suggests early biosphere oxygenation. *Nat Ecol Evol* 5:442–448.

Jackson TA (2015) Ultraviolet radiation-absorbing ''Humic Pigments'' of cyanobacteria in microbial mats: their presumptive photoprotective function and relevance to early precambrian microbial ecology and evolution. *Geomicrobiol J* 32:420–432.

Javaux EJ (2019) Challenges in evidencing the earliest traces of life. *Nature* 572:7770 451–460.

Jehlička J, Edwards HGM, and Oren A (2014) Raman spectroscopy of microbial pigments. *Appl Environ Microbiol* 80: 3286– 3295.

Jones MR, Pinto E, Torres MA, *et al*. (2021) CyanoMetDB, a comprehensive public database of secondary metabolites from cyanobacteria. *Water Res* 196:117017.

Kim S, Chen J, Cheng T, *et al*. (2019) PubChem 2019 update: improved access to chemical data. *Nucleic Acids Res* 47: D1102–D1109.

Kind T and Fiehn O (2007) Seven Golden Rules for heuristic filtering of molecular formulas obtained by accurate mass spectrometry. *BMC Bioinformatics* 8:105.

Knoll AH and Golubic S (1992) Proterozoic and living cyanobacteria. In *Early Organic Evolution: Implications for Mineral and Energy Resources,* edited by P. Schidlowski, M. Golubic, S. Kimberley, M. McKirdy, and D. Trudinger, Springer Verlag, Berlin, pp 450–462.

Kwok S (2017) Abiotic synthesis of complex organics in the Universe. *Nat Astron* 1:642–643.

Lamprinou V, Skaraki K, Kotoulas G, *et al*. (2013) A new species of *Phormidium*; (Cyanobacteria, Oscillatoriales) from three Greek Caves: morphological and molecular analysis. *Fundam Appl Limnol* 182:109–116.

Lara Y, Durieu B, Cornet L, *et al*. (2017) Draft genome sequence of the axenic strain *Phormidesmis priestleyi* ULC007, a cyanobacterium isolated from Lake Bruehwiler (Larsemann Hills, Antarctica). *Genome Announc* 5:7.

Lepot K, Compère P, Gérard E, *et al*. (2014) Organic and mineral imprints in fossil photosynthetic mats of an East Antarctic lake. *Geobiology* 12:424–450.

Lukas KJ and Hoffman EJ (1984) New endolithic cyanophytes from the North Atlantic Ocean. III *Hyella pyxis* LUKAS & HOFFMAN sp. nov. *J Phycol* 20:515–520.

Manojlovic NT, Vasiljevic PJ, Gritsanapan W, *et al*. (2010) Phytochemical and antioxidant studies of *Laurera benguelensis* growing in Thailand. *Biol Res* 43:169–176.

McCollom TM and Simoneit BRT (1999) Abiotic formation of hydrocarbons and oxygenated compounds during thermal decomposition of iron oxalate. *Orig Life Evol Biosph* 29: 167–186.

McMahon S and Cosmidis J (2021) False biosignatures on Mars: anticipating ambiguity. *J the Geol Soc* 2021:jgs2021-050.

Ménez B, Pisapia C, Andreani M, *et al*. (2018) Abiotic synthesis of amino acids in the recesses of the oceanic lithosphere. *Nature* 564:59–63.

Moore KR, Magnabosco C, Momper L, *et al*. (2019) An expanded ribosomal phylogeny of cyanobacteria supports a deep placement of plastids. *Front Microbiol* 10:1612.

Movasaghi Z, Rehman S, and Rehman IU (2007) Raman spectroscopy of biological tissues spectroscopy of biological tissues. *Appl Spectrosc Rev* 42:493–541.

Nägeli C and Schwendener S (1877) The Microscope: Theory and application (pp. xii, 679 p.). W. Engelmann. https://catalog.hathitrust.org/Record/001995316

Němečková K, Culka A, Němec I, *et al.* (2021) Raman spectroscopic search for scytonemin and gloeocapsin in endolithic colonizations in large gypsum crystals. *J Raman Spectrosc* 2021:jrs.6186.

Numata Y and Tanaka H (2011) Quantitative analysis of quercetin using Raman spectroscopy. *Food Chem* 126:751–755.

Ostrander CM, Johnson AC, and Anbar AD (2021) Earth's first redox revolution. *Annu Rev Earth Planet Sci* 49:337–366.

Ouyang Q, Zhou CM, Pang K, *et al.* (2021) Silicified *Polybessurus* from the Ediacaran Doushantuo Formation records microbial activities within marine sediments. *Palaeoworld* [Epub ahead of print]; DOI: 10.1016/j.palwor.2021.03.001.

Pawlowska MM, Butterfield NJ, and Brocks JJ (2013) Lipid taphonomy in the Proterozoic and the effect of microbial mats on biomarker preservation. *Geology* 41:103–106.

Pentecost A (2014) Distribution and ecology of cyanobacteria in the rocky littoral of an English Lake District water body, Devoke water. *Life* 4:1026–1037.

Pentecost A and Whitton BA (2012) Subaerial cyanobacteria. In *Ecology of Cyanobacteria II*, edited by B.A. Whitton, Springer, Netherlands, pp 291–316.

Pompeu DR, Larondelle Y, Rogez H, *et al*. (2018) Characterization and discrimination of phenolic compounds using Fourier transform Raman spectroscopy and chemometric tools. *Biotechnol, Agronom Soc Environ* 22:13–28.

Proteau PJ, Gerwick WH, Garcia-Pichel F, *et al*. (1993) The structure of scytonemin, an ultraviolet sunscreen pigment from the sheaths of cyanobacteria. *Experientia* 49:825–829.

Raabová L, Kovacik L, Elster Josefâ, *et al*. (2019) Review of the genus *Phormidesmis* (Cyanobacteria) based on environmental, morphological, and molecular data with description of a new genus *Leptodesmis*. *Phytotaxa* 395:1–16.

Radtke G and Golubic S (2011) Microbial euendolithic assemblages and microborings in intertidal and shallow marine habitats: insight in cyanobacterial speciation. I*n Advances in Stromatolite Geobiology,* edited by J. Reitner; N.-V. Quéric, and G. Arp, Springer-Verlag, Berlin, pp 233–263.

Rippka R, Deruelles J, Waterbury JB, *et al*. (1979) Generic assignments, strain histories and properties of pure cultures of cyanobacteria. *Microbiology* 111:1–61.

Sanger JE (1988) Fossil pigments in paleoecology and paleolimnology. *Palaeogeogr Palaeoclimatol Palaeoecol* 62:343–359.

Sergeev VN, Sharma M, and Shukla Y (2012) Proterozoic fossil cyanobacteria. *Palaeobotanist* 61:189–358.

Simionescu CI, Simionescu BC, Mora R, *et al*. (1978) Porphyrin-like compounds genesis under simulated abiotic conditions. *Orig Life* 9:103–114.

Singh DP, Prabha R, Verma S, *et al*. (2017) Antioxidant properties and polyphenolic content in terrestrial cyanobacteria. *3 Biotech* 7:2134.

Sivonen K, Leikoski N, Fewer DP, *et al*. (2010) Cyanobactins—ribosomal cyclic peptides produced by cyanobacteria. *Appl Microbiol Biotechnol* 86:1213–1225.

Socha AM, Garcia D, Sheffer R, *et al*. (2006) Antibiotic bisanthraquinones produced by a streptomycete isolated from a cyanobacterium associated with *Ecteinascidia turbinata*. *J Nat Prod* 69:1070–1073.

Soule T, Stout V, Swingley WD, *et al*. (2007) Molecular genetics and genomic analysis of scytonemin biosynthesis in *Nostoc punctiforme* ATCC 29133. *J Bacteriol* 189:4465–4472.

Storme J-Y, Kleinteich J, Wilmotte A, *et al*. (2015) Raman characterization of the UV-protective pigment gloeocapsin and its role in the survival of cyanobacteria. *Astrobiology* 15: 843–857.

Sturdy M, Krunic A, Cho S, *et al*. (2010) Eucapsitrione, an anti-*Mycobacterium tuberculosis* Anthraquinone derivative from the cultured freshwater cyanobacterium *Eucapsis* sp. *J Nat Prod* 73:1441–1443.

Taton A, Grubisic S, Ertz D, *et al*. (2006) Polyphasic study of Antarctic cyanobacterial strains. *J Phycol* 42:1257–1270.

Varnali T, Edwards HGM, and Hargreaves MD (2009) Scytonemin: molecular structural studies of a key extremophilic biomarker for astrobiology. *Int J Astrobiol* 8:133–140.

Vincent WF (2000) Cyanobacterial dominance in the polar regions. In *The Ecology of Cyanobacteria: Their Diversity in Time and Space,* edited by B.A. Whitton and M. Potts, Kluwer Academic Publishers, Dordrecht, the Netherlands, pp 321–340.

Vinnichenko G, Jarrett AJM, Hope JM, *et al*. (2020) Discovery of the oldest known biomarkers provides evidence for phototrophic bacteria in the 1.73 Ga Wollogorang Formation, Australia. *Geobiology* 18:544–559.

Vogel E and Kiefer W (1998) Investigation of the metal adsorbate interface of the system silver coumarin and silver hydrocoumarin by means of surface enhanced Raman spectroscopy. *Fresenius J Anal Chem* 361:628–630.

Wood BR, Quinn MA, Tait B, *et al*. (1998) FTIR microspectroscopic study of cell types and potential confounding variables in screening for cervical malignancies. *Biospectroscopy* 4:75–91.

Wynn-Williams DD, Edwards HGM, Newton EM, *et al*. (2002) Pigmentation as a survival strategy for ancient and modern photosynthetic microbes under high ultraviolet stress on planetary surfaces. *Int J Astrobiol* 1:39–49.

Żyszka-Haberecht B, Niemczyk E, and Lipok J (2019) Metabolic relation of cyanobacteria to aromatic compounds. *Appl Microbiol Biotechnol* 103:1167–1178.

Address correspondence to:
Yannick J. Lara
Early Life Traces & Evolution–Astrobiology
UR Astrobiology
University of Liège
Liège 4000
Belgium

E-mail: ylara@uliege.be

Emmanuelle J. Javaux
Early Life Traces & Evolution–Astrobiology
UR Astrobiology
University of Liège
Liège 4000
Belgium

E-mail: ej.javaux@uliege.be

Submitted 6 May 2021
Accepted 21 January 2022
Associate Editor: Don Cowan

Abbreviations Used

AOE = Archean oxygenation events
ESI = electrospray ionization
FT-IR = Fourier-transform infrared
GOE = Great Oxidation event
HPLC = high-pressure liquid chromatography
LCMS = liquid chromatography–mass spectrometry
rdb = ring and double bond
R-HCA = R-mode hierarchical cluster analysis
ROS = reactive oxygen species
RT = retention time
UV = ultraviolet